Science of the Total Environment 951 (2024) 175439

Contents lists available at ScienceDirect

Science of the Total Environment

journal homepage: www.elsevier.com/locate/scitotenv

Groundwater–rock interactions and mixing in fault–controlled karstic aquifers: A structural, hydrogeochemical and multi-isotopic review of the Pontina Plain (Central Italy)

Francesca Gori [a], Marino Domenico Barberio [b], Maurizio Barbieri [c], Tiziano Boschetti [d], Giovanni Luca Cardello [e,*], Marco Petitta [a]

[a] Department of Earth Sciences, Sapienza University of Rome, Italy
[b] National Institute of Volcanology and Geophysics, Rome, Italy
[c] Department of Chemical Engineering and Environmental Materials, Sapienza University of Rome, Italy
[d] Department of Chemistry, Life Sciences and Environmental Sustainability, University of Parma, Italy
[e] Department of Chemistry, Physics, Mathematics and Natural Sciences, University of Sassari, Italy

HIGHLIGHTS

- Structural and hydrogeochemical insights reveal processes in faulted karst aquifers.
- Diverse geochemical processes shape groundwater composition at deep and shallow depth.
- Mixing of Ca–HCO_3 from karst with Na–Cl waters react with evaporite and silicates.
- Water-rock interaction and mixing occur on the fault edging of the Pontina Plain.
- A new pollucite and analcime activity geothermometer is proposed.

GRAPHICAL ABSTRACT

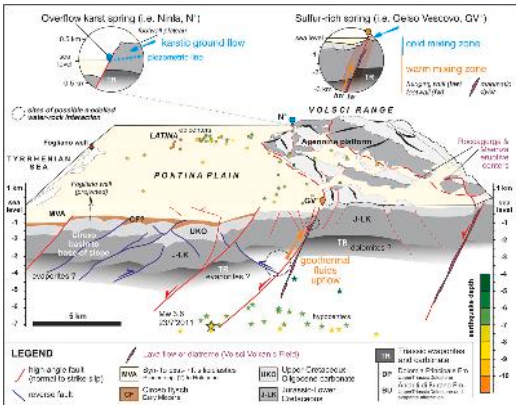

ARTICLE INFO

Editor: Christian Herrera

Keywords:
Hydrogeochemistry
Isotopes
Groundwater mixing
Water–rock interaction
Karstic aquifers
Fault

ABSTRACT

Karstic aquifers represent crucial water resources and are categorized as either stratigraphically or fault–controlled. This study investigates groundwater–rock interactions and mixing processes within one of the largest fault–controlled karstic aquifers in Central Italy, adjacent to the Pontina plain, which is a highly populated area where agricultural activities and climate change challenge the groundwater assessment of a complex aquifer. We conducted structural, hydrogeochemical, and multi-isotopic screening of ten selected springs with different degrees of mineralization (ranging from Ca–HCO_3 to Na–Cl hydrofacies), incorporating new analyses and modeling of $\delta^{34}S(SO_4)$, $\delta^{18}O(SO_4)$, $^{87}Sr/^{86}Sr$, and $\delta^{11}B$. Additionally, the reinterpretation of a seismic section provides a more detailed framework extending to depths of approximately 5–7 km that allows the identification of the geometry of normal faults, which act as pathways for upwelling fluids. Our findings reveal that

* Corresponding author.
E-mail address: glcardello@uniss.it (G.L. Cardello).

https://doi.org/10.1016/j.scitotenv.2024.175439
Received 24 May 2024; Received in revised form 18 July 2024; Accepted 8 August 2024
Available online 17 August 2024

hydrogeochemical compositions result from multiple interactions between karstic water and deeper fluids that have interacted with different rocks. Concentration (Na/Li) and isotope (SO_4–H_2O) geothermometers, coupled with geochemical modeling and trace element analysis, enabled the estimation of a water temperature equilibrium of approximately 95.5 °C, with Triassic evaporites generally corresponding to a depth of approximately 3 km and a temperature of 40 °C with magmatic rocks at approximately 1 km depth, which is likely associated with ongoing tectonics and the Quaternary tectonically controlled Volsci Volcanic Field. To obtain the latter estimate, we used a new geothermometer activity based on the equilibrium between analcime and pollucite. Furthermore, this multidisciplinary approach enhances the understanding of groundwater behavior in fault–controlled karstic aquifers, where mantle-derived CO_2 dissolved in groundwater is the driving force behind water–rock interactions. Given the potential for further variations in mixing, which may worsen water quality and increase aquifer vulnerability, periodic monitoring of these processes is essential in a human-impacted environment amidst ongoing climate change.

1. Introduction

Karstic aquifers consist of strategic water resources sensitive to groundwater hydrogeochemical variations, whose vulnerability depends on their geological background, their use, and climatic variations (e.g., Barbieri et al., 2023; Moreno-Gómez et al., 2023; Deng et al., 2024; Zhang et al., 2024). They are high-permeability and high-porosity groundwater systems characterized by the dissolution of soluble carbonate rocks, resulting in distinctive landforms and underground drainage networks (Taniguchi et al., 2003; Bakalowicz, 2005; Ford and Williams, 2007). We categorize karstic aquifers into two main types on the basis of their controlling geological features: stratigraphically controlled and fault–controlled (Fig. 1).

In stratigraphically controlled karstic aquifers, the development and distribution of karst features are primarily determined by the lithologic properties and stratigraphic architecture of the bedrock. In contrast, in fault–controlled karstic aquifers, the influence of faults dramatically influences the development of karst features. In particular, high-angle faults act as conduits for groundwater flow and can lead to upwelling of deep thermal fluids (Faulds et al., 2006; Jolie et al., 2015; Torresan et al., 2020; Buttitta et al., 2023).

Defining the origin and evolution of groundwater stands as a critical endeavor in hydrogeological investigations, particularly in carbonate-dominated fold-and-thrust belts, where karstic stratified aquifers and tectonic discontinuities intricately govern fluid dynamics (Goldscheider et al., 2010; Bense et al., 2013; Smeraglia et al., 2016). The integration of structural, hydrogeochemical and environmental isotopic data has emerged as an indispensable tool for reconstructing hydrogeological pathways (Barbieri et al., 2005; Yang et al., 2019; Medici et al., 2023; Lorenzi et al., 2024), identifying recharge zones (Liu and Yamanaka, 2012; Sappa et al., 2018), estimating fluid temperatures in both current (Wang et al., 2015; Vespasiano et al., 2021; Boschetti et al., 2022) and fossil settings (Lacroix et al., 2018; Cardello et al., 2024), and elucidating the extent of mixing among different groundwater sources (Duchi et al., 1991; Barbieri et al., 2017). Such efforts have culminated in a comprehensive and comparative analysis crucial for defining hydrogeological models and leveraging hydrogeochemical signatures encompassing chemical–physical parameters in regard to both concentrations of major ions and trace elements and isotope ratios. Advancements in analytical techniques in recent years have made analyses more powerful, facilitating the refinement of existing hydrogeological models, including water–rock interactions, as well as heating and mixing processes (Piscopo et al., 2006; Goldscheider et al., 2010; Petitta et al., 2011; Doummar et al., 2012; Aydin et al., 2020; Li et al., 2020; Barberio et al., 2021; Bojar et al., 2021; Gori et al., 2023).

In this study, we review the structural setting and groundwater–rock interactions in the Pontina Plain, a coastal plain situated south of the Colli Albani volcano and on the western edge of the northern part of the Volsci Range (Lepini Mounts and Seiano Mount). The Pontina Plain has one of the major karst fault-bounded aquifers in Central Italy (Fig. 2). Similar to what has been recognized in the southern part of the Volsci Range (Sappa et al., 2012; Saroli et al., 2017, 2019), Boni et al. (1980) documented different types of springs, varying in temperature and chemical composition from cold karstic to hypothermal sulfur-rich and highly conductive springs, whose mixing has sparked different interpretations, possibly evoking, among other factors, the role of a fault-related magmatic system.

Previous hydrogeological and geochemical characterizations have

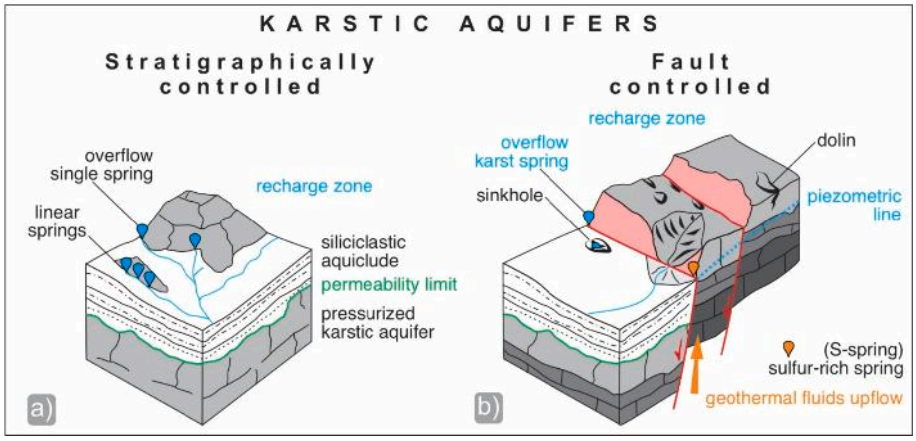

Fig. 1. Sketches summarizing the morphological, structural, and hydrogeological characteristics of stratigraphically controlled (a) and fault–controlled (b) karstic aquifers with nomenclature from Civita (1972) and Keegan-Treloar et al. (2022). The orange arrow indicates the upwelling of potentially deep thermal fluids, which may mix with less mineralized and cold karstic waters in light blue. In light of current climate change and anthropic pressure on water resources, a decrease in aquifer recharge can induce significant hydrogeochemical changes in karstic carbonate aquifers, increasing the contribution of geothermal fluids to potential environmental and management issues.

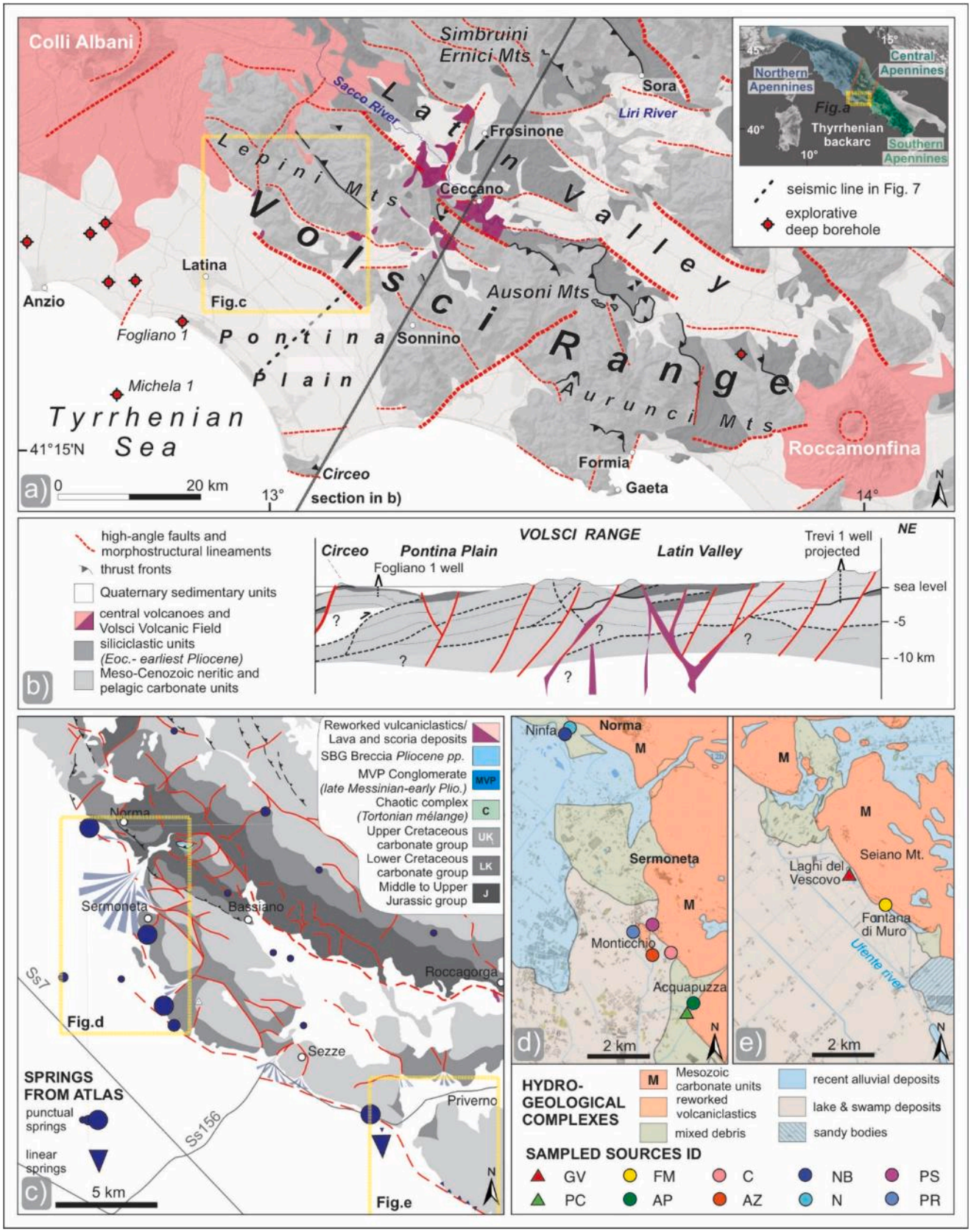

Fig. 2. a) Tectonic simplified map of southern Latium (modified after Cardello et al., 2021). The location is outlined in the inset on the top right of the figure. b) Crustal sketch cross-section with thrusts in blue and normal faults in red (modified after Mostardini and Merlini, 1988), whose location is outlined in a). c) Geological map of the western Lepini Mounts and minor carbonate reliefs (modified from Cardello et al., 2021) with spring locations from Capelli et al. (2012). The location is outlined in a). d-e) Detailed hydrogeologic maps (from https://sit.provincia.latina.it/) showing the locations of the springs sampled in this work.

highlighted the presence of karstic shallow groundwater flow and mixed hydrothermal flow (Bono, 1981; Tuccimei et al., 2005), with alternative hypotheses suggesting influences ranging from volcanic to evaporitic source zones (Boni et al., 1980). As recently demonstrated (Cardello et al., 2020; Marra et al., 2021), Pleistocene monogenetic volcanism has utilized high-angle fault systems crossing karst terrains. Consequently, to test the presence of a volcanic contribution to groundwater, there is a need for geochemical and multi-isotopic characterization to assess fluid flow pathways effectively. To address the processes and sites of mixing, a multiscale integrated interdisciplinary approach was undertaken. This highlights the need for continuous monitoring and groundwater management while considering ongoing climate change and anthropic pressure on water resources.

We utilized this emblematic area as a world-class example of a "fault–controlled mixed groundwater karstic aquifer". In particular, this study integrated field structural observations and reinterpretation of subsurface data with newly collected hydrogeochemical and isotopic data from ten springs at the piedmont of the northern Volsci Range (Fig. 2), including parameters such as $\delta^{18}O(H_2O)$, $\delta^{2}H(H_2O)$, $\delta^{34}S(SO_4)$, $\delta^{18}O(SO_4)$, $^{87}Sr/^{86}Sr$, and $\delta^{11}B$, which act as natural tracers to define hydrogeological and hydrogeochemical water–rock interaction processes and pathways.

Through geochemical modeling, thermodynamics, and statistical calculations, we estimated the temperature of the mixing sites within the subsurface, with insights into the mixing processes between two groundwater systems: i) shallow Ca–HCO_3 groundwater circulating in a regional karstic aquifer and ii) deep Na–HCO_3–Cl groundwater with saline and thermal features. The findings contribute to the definition of the depths of mixing interactions within a typical fault–controlled mixed groundwater karstic aquifer, with practical implications for sustainable water resource management, risk of sinkhole formation (Bono, 1995; Salvati and Sasowsky, 2002; Sappa and Coviello, 2012) and active tectonics.

2. Geological and hydrogeological setting

2.1. Regional geology

The Apennines exhibit evolutionary patterns similar to those of many Alpine–Himalayan fold-and-thrust belts (Cloetingh et al., 2004; Carminati and Doglioni, 2012; Schmid et al., 2020). Preserving a low- to nonmetamorphic diagenetic status, this belt retains records of carbonate platform to basin (Tethyan) and siliciclastic successions (Cardello et al., 2022 and references therein). The regional stratigraphic architecture reflects passive processes from the Late Triassic–Early Jurassic rift to Cretaceous basinal development (Accordi et al., 1988; Cardello and Doglioni, 2015; Tavani et al., 2021). The accretion of these inherited passive margin units atop the subducting Adria Plate occurred in the Neogene, which was driven by the E/NE-ward migration of frontal thrusts. These processes gave rise to deep and wedge-top dynamics (Cardello et al., 2021). From the Pliocene onward, the western part of the Apennine fold-and-thrust belt experienced crustal stretching with back-arc extension of the crust.

In contrast to the persistent platform carbonate in the Volsci Range (VR, Fig. 2a), subsurface information indicates that a base-of-slope to carbonate basinal succession exists beneath the Pontina Plain. Toward the present-day offshore to the west, Triassic evaporites are present (Fig. 2b) (see Section 5.1). This geometry reflects an inherited Tethyan passive margin physiography, which was reshaped during the Pliocene–Pleistocene extension of the Tyrrhenian margin. Afterward, throughout the Pleistocene, volcanism migrated southeastward. Moreover, coastal plains exhibit widespread travertine deposits, which are typically associated with hydrothermal activity and deep degassing CO_2 of mantle origin (Minissale, 2004; Chiodini et al., 2004; Carapezza et al., 2012; Cuoco et al., 2017), resulting in tectonically controlled thermal springs on the surface.

The VR comprises smaller mountain groups, namely, the West and East Lepini Mounts, the Seiano Mount, the Ausoni Mounts, and the West and East Aurunci Mounts (Fig. 2) (Saroli et al., 2017, 2019). The VR exposes a 2.5 km thick succession of Jurassic to Cretaceous shallow-water carbonates, which rest on top of a few-hundred-meters-thick Triassic dolostone. The VR carbonate succession is topped by Middle to Upper Miocene synorogenic marly and siliciclastic rocks that occur at the footwall of thrusted carbonate units (Angelucci, 1966; Cosentino et al., 2002; Centamore et al., 2007; Cardello et al., 2021) (Fig. 2c).

Postemersion erosional terraces occur at various elevations (Centamore et al., 2007; Servizio Geologico d'Italia, 2010), possibly reflecting late to postorogenic tectonics. During the Late Pliocene, the VR experienced uplift, while the blocks thrown down toward the southwest were invaded by seawater (Tavani et al., 2021 and references therein). In the VR, beginning in the Early Pleistocene, uplift was accompanied by normal faulting, which gave rise to a horst-and-graben structure with fault-bounded marine to continental basins inland (Servizio Geologico d'Italia, 2010). The Pleistocene successions also contain volcaniclastic units from nearby volcanoes (Sevink et al., 2020; Alessandri et al., 2021). Over the past 800 k years, first-order high-angle faults in the VR have experienced rooted volcanic activity, locally marked by tens of monogenetic eruptive centers (Cardello et al., 2020; Marra et al., 2021). Furthermore, some faults are locally affected by neotectonic movements, such as in the Ausoni Mounts, edging the Pontina Plain (Alessandri et al., 2021), where earthquakes of low magnitude ($M_w \leq 4.4$; Rovida et al., 2020) have occurred.

2.2. Background on karst development

Large-scale epigeous karst forms include plateaus and endorheic basins, whereas smaller-scale forms such as karstic valleys, poljes, and dolines are accompanied by a complex underground system of vertical shafts and caves (Servizio Geologico d'Italia, 2010), which typically align with fault zones (Agostini, 1992). These forms are occasionally flooded, caves are partially sealed by speleothems, and springs are locally associated with travertine occurrences. Karstic alteration in the VR likely started during the Cretaceous emersions and continued into the Paleocene before the platform was covered with basinal sedimentation (Servizio Geologico d'Italia, 2010). Following the Tortonian–Messinian mountain buildup between approximately 12 and 6 Ma, the highest VR thrust sheets underwent massive erosion, which intensified during the salinity crisis (Cardello et al., 2021 and references therein), whereas the eastern part of the Apennines still developed under submarine conditions. Between 5.5 and 4.5 Ma, the VR carbonates underwent further exhumation (Fellin et al., 2022). According to the average uplift history of the nearby Simbruini Mounts (Fig. 2; Delchiaro et al., 2021), from the Late Pliocene, the area experienced uplift ranging from approximately 690–370 m Ma^{-1} (Delchiaro et al., 2021). This uplift interacted with the horst-and-graben setting of the normal fault system with NW-, ENE- and (N)NE-striking high-angle faults oblique to normal faults (Servizio Geologico d'Italia, 2010; Alessandri et al., 2021), influencing the distributions of 1) Quaternary deposits, 2) karst forms, and 3) fluid circulation. Given the presence of paleokarst at depths of approximately 100–300 m below sea level in the hanging wall of the fault bordering the Pontina Plain (Federici, 1979; Agostini, 1992), karst development was likely influenced by tectonics and climatic variations. Sinkhole occurrence is limited to a narrow strip between the western border of the VR and the S.S.7 Appia freeway, and their distribution has been related to the slow dissolution of the buried carbonate bedrock due to CO_2-rich fluids, which migrate through major fault zones (Salvati and Sasowsky, 2002; Tuccimei et al., 2005).

2.3. Hydrogeological, subsurface setting and climate

Among the three different groups of ridges located in the VR, the Lepini Mounts host a regional karst aquifer classified as "unconfined

with an undefined bottom surface" (Fig. 2d-e), whose base level lies at the northeastern edge of the Pontina Plain, with a mean annual discharge as high as 15 m^3/s (Boni et al., 1980; Sappa et al., 2014).

The hydrogeological unit is represented by carbonates), whose groundwater recharge occurs through karst fissures, generating a mean recharge rate higher than 800 mm/yr. Infiltration is driven primarily by fractured carbonates, with dolostones and marly horizons generating secondary circuits. Spring discharges clearly lack an intersection between the karst network and springs (Boni et al., 1980; Petitta, 1994), which is likely due to the highly heterogeneous permeability (transmissivity values ranging from 1×10^{-1} to 9×10^{-5} m^2/s) and the hydraulic gradient (5–6 m/km). In the backbone of the Lepini Mounts, the saturated zone of the aquifer lies >1000 m below the surface. This hydrogeologic unit continues beneath the Pontina Plain, where it is downfaulted and covered by terrigenous and a few tens of meters-thick cover of volcaniclastic deposits (Boni et al., 1980). At the boundary between the Pontina Plain and the VR (i.e., at the piedmont of the Lepini Mounts and Seiano Mount.; Fig. 2d-e), most groundwater emerges in numerous aligned springs with different hydrogeochemical features. Despite the Pontina Plain being generally between 0 and 40 m above sea level, the Quaternary alluvial and fluvial-coastal facies deposits are up to several hundred meters thick, implying high subsidence and/or tectonics in the so-called "Pontina graben" (Boni et al., 1980; Serva and Brunamonte, 2007). Although geological and hydrogeological models have been proposed in the past (Boni et al., 1980; Bono, 1981), seismic data (www.videpi.com) were acquired only by the petroleum company AGIP (Azienda Generale Italiana Petroli) in 1986. Although these sections were variably interpreted through the years by Mostardini and Merlini (1988), Milia and Torrente (2015); Milia et al. (2017) and Tavani et al. (2023), their interpretations were not designed or integrated into hydrogeological and hydrogeochemical studies. The climate of the study area is characterized by rainy autumn winters and dry summers. Thus, recharge of the Lepini carbonate aquifer occurs mostly during autumn and winter. Specifically, according to the Köppen–Geiger climate classification (Köppen and Geiger, 1930), the meteorological conditions are recognized as "hot-summer Mediterranean climate" (Csa type).

3. Materials and methods

3.1. Structural data

We conducted this study on the basis of a new structural–geological survey of the carbonate substrate of the fault edging the Pontina Plain, which integrated previous work (e.g., Geological Map of Italy; Accordi, 1966; Cardello et al., 2020, 2021). To elucidate fault kinematics, we conducted field surveys, capturing measurements of folds, faults, bedding fractures, and slicken fibers at key locations. We processed these data via TectonicsFP software (Ortner et al., 2002), which employs lower hemisphere projections and rose diagrams for visualization. Gray circles represent the planes between the principal and minimal eigenvectors. Notably, an eigenvector is a vector that undergoes stretching but not rotation when subjected to matrix operations. Wells and seismic lines are publicly available at www.videpi.com (last accessed on 10 April 2024).

3.2. Sampling and hydrogeochemical analyses

To define the hydrogeochemical features of groundwater on the Pontina Plain, we selected 10 of the most representative springs: Ninfa, Ninfa Bambù, Polla Saverio, Cartiera, Acquapuzza, Polla Catena, Polla Regina, Fontana di Muro, and Gelso Vescovo, hereafter reported with their respective IDs (Table 1) (Fig. 2d-e).

We carried out sampling surveys for the measurement of chemical–physical parameters and the collection of groundwater samples for hydrogeochemical and isotopic analyses in 2020 and 2021.

Table 1
Chemical-physical parameters, major ions, and minor elements used in the discussion section (for the concentrations of all the trace elements the reader is referred to Supplementary Material 3) of the springs from the study area (sample ID corresponds to the sites displayed in Fig. 2d-e).

Sample name	Sample id	Sampling date	T	EC	pH	TDS	Ca	Mg	Na	K	Cl	SO_4	HCO_3	F	NO_3	SiO_2	Li	B	Rb	Sr	Cs
		(dd/mm/yy)	°C	μS/cm		mg/l	mg/l	mg/l	mg/l	mg/l	mg/l	mg/l	mg/l	mg/l	mg/l	mg/l	μg/l	μg/l	μg/l	μg/l	μg/l
SRG Gelso Vescovo	GV	30/01/20	19.1	4800	6.62	2979	293	85.4	703	19.3	1480	164	463	0.50	–	16	33.46	384.60	34.12	1015.00	16.39
SRG Gelso Vescovo	GV	19/10/20	19.0	3690	6.82	2575	335	83.4	493	31.5	1174	184	543	0.50	–	–	21.24	238.90	21.88	1031.00	9.10
SRG Gelso Vescovo	GV	12/02/21	18.4	4370	6.78	–	–	–	–	–	–	–	–	–	–	–	24.36	370.10	21.24	2542.00	8.33
Cartiera	C	30/01/20	15.1	805	7.08	496	128	25.9	24.5	4.53	35.53	33.7	487	0.27	–	–	4.02	72.45	7.49	236.70	0.67
Cartiera	C	19/10/20	15.1	748	7.06	451	108	24.1	29.2	4.38	30.78	29.7	441	0.04	3.06	–	5.75	88.91	10.49	471.10	1.32
Acqua Zolfa	AZ	30/01/20	14.3	881	6.88	555	160	28.4	12.7	4.87	15.64	29.5	606	0.26	–	8.57	5.64	85.75	10.09	283.00	1.76
Acqua Zolfa	AZ	19/10/20	14.3	762	7.01	453	124	24.1	12.8	6.03	17.12	29.0	475	0.18	1.23	–	4.06	55.39	9.35	383.60	1.03
Polla 1 Catena	PC	30/01/20	16.3	2100	6.91	1117	146	34.4	223	11.6	435.9	72.5	385	0.22	–	10.5	9.06	148.60	16.50	431.20	2.08
Polla 1 Catena	PC	19/10/20	16.3	2100	6.96	1360	135	38.8	321	10.2	605.0	91.3	317	–	–	–	4.13	62.47	7.52	356.80	0.65
Polla 1 Catena	PC	12/02/21	16.3	2050	6.97	–	–	–	–	–	–	–	–	–	–	–	8.78	182.50	12.70	1164.00	1.44
Ninfa Bambù	NB	30/01/20	13.4	458	7.47	261	77.2	11.6	7.27	1.87	9.521	4.32	289	0.13	4.84	–	1.41	21.93	9.94	154.00	0.35
Ninfa Bambù	NB	19/10/20	13.6	463	7.43	261	74.2	12.7	7.44	1.75	16.45	5.78	269	0.09	7.42	–	1.16	16.88	7.68	167.10	0.28
Ninfa	N	30/01/20	12.9	421	7.53	237	69.1	12.5	5.58	0.810	8.58	3.52	267	0.06	3.36	4.56	0.65	16.77	3.92	130.00	0.24
Ninfa	N	19/10/20	13.2	412	7.56	229	64.4	13.4	5.21	0.637	12.91	4.86	246	0.05	3.84	–	0.57	12.30	3.19	120.60	0.15
Fontana di Muro	FM	30/01/20	15.0	1088	7.19	660	115	25.1	99.7	4.19	185.8	35.1	378	0.21	5.17	–	3.83	55.60	7.25	307.20	1.25
Fontana di Muro	FM	19/10/20	15.1	1092	7.23	642	108	26.7	95.3	5.44	209.8	35.3	314	0.14	4.17	–	1.78	25.35	3.46	278.70	0.60
Fontana di Muro	FM	12/02/21	15.0	1048	7.26	–	–	–	–	–	–	–	–	–	–	–	3.70	80.04	5.31	702.20	0.76
Acquapuzza	AP	30/01/20	15.2	1241	6.87	817	172	32.7	88.5	11.2	152.3	57.2	605	0.86	–	9.71	7.10	108.70	12.39	339.10	1.99
Acquapuzza	AP	12/02/21	15.2	1187	6.92	859	204	32.3	92.1	9.97	205.3	34.2	549	0.25	5.24	–	6.95	137.60	9.82	892.60	1.38
Polla Saverio	PS	30/01/20	14.3	776	6.99	468	133	26.8	7.87	3.32	9.837	31.5	510	0.25	–	–	4.47	69.25	8.81	241.90	1.77
Polla Saverio	PS	19/10/20	14.3	766	7	351	79.6	29.3	9.69	4.89	16.3	35.5	349	0.23	0.38	–	3.91	54.42	8.78	362.20	1.57
Polla Regina	PR	30/01/20	14.1	710	7.11	433	126	21.0	9.53	5.02	9.457	23.8	473	0.21	1.78	–	3.71	57.41	9.97	257.70	0.94

We performed measurements of pH, electrical conductivity (EC), and temperature (T) onsite with the multiparametric WTW Multi 3420 probe with accuracies of ±0.01 pH units, ±1 μS/cm, and ±0.1 °C, respectively. We filtered groundwater samples in situ with a 0.45 μm filter into polyethylene bottles and stored them at low temperatures to avoid alterations in their components. After field filtering, we acidified in situ samples for the analyses of cations, both major and trace, to 1 % *v*/v, adding 1 ml of 65 % HNO_3 Suprapur® (Supelco).

For the determination of major ions (i.e., anionic and cationic contents), we analyzed samples by ion chromatography at the Geochemistry Laboratory of the Department of Earth Sciences at Sapienza University of Rome (Italy). We used Dionex ICS-5000 and Dionex ICS-1100 chromatographs to analyze anions (F^-, Cl^-, SO_4^{2-}, and NO_3^-; Standard Method 4110; Baird et al., 2017) and cations (Ca^{2+}, Mg^{2+}, Na^+, and K+; Method 3030; APAT-IRSA-CNR, 2003), respectively. We measured the carbonate alkalinity as HCO_3^- by titration with a 0.05 N HCl solution and a dye indicator (Standard Method 2320-B; Baird et al., 2017); the precision was ±6 mg/l and the accuracy was ±11 mg/l. We analyzed the dissolved silica as SiO_2(aq) at the SCVSA Department, University of Parma (Italy) using the heteropoly blue spectrophotometric method (Standard Method 4500-SiO_2 D; Baird et al., 2017), a Spectroquant® cuvette reagents test kit and a PHARO 300 UV/VIS spectrophotometer (Merck Millipore, Burlington, MA, USA); the precision was ±0.09 mg/l, with an accuracy of ±0.2 mg/l. In accordance with Standard Method 1030E for checking the correctness of analyses (Baird et al., 2017), we checked for ionic balance errors ≤5 % for each sample.

We analyzed dissolved minor and trace element concentrations (Li, B, Al, V, Cr, Mn, Fe, Co, Ni, Cu, Zn, Ga, As, Rb, Sr, Mo, Cd, In, Sn, Sb, Cs, W, Hg, Pb, and U) using an ICP-MS (X Series 2 Thermo-Fisher Scientific Waltham, MA, USA; Standard Method 3125; Baird et al., 2017). We prepared blanks, standard solutions, and sample dilutions via ultrapure water (Millipore, Milli-Q, 16 MW cm), and we used an internal standard, Rh, to correct the ICP–MS instrument drift. The analytical accuracy of this method ranges between 2 % and 5 %.

We carried out isotopic measurements of the stable isotopes of water molecules, $\delta^{18}O(H_2O)$ and $\delta^{2}H(H_2O)$, at the University of Parma. We analyzed hydrogen and oxygen stable isotopes in water using an automatic equilibration device (Finnigan HDO) in line with a Finnigan Delta Plus mass spectrometer (Boschetti et al., 2005; Longinelli and Selmo, 2003). The $\delta^{2}H(H_2O)$ was evaluated by directly equilibrating hydrogen gas with water by means of a platinum catalyst (Horita and Kendall, 2004); determination of $\delta^{18}O(H_2O)$ was performed on CO_2 gas equilibrated with water at 18 ± 0.1 °C. We measured all the samples at least twice, and we reported the value of the mean of two consistent results. All the measurements were carried out against laboratory standards that were periodically calibrated against the international isotope water reference materials recommended by the IAEA (V-SMOW2 and SLAP2). The standard error (2σ) was within ±0.08 to ±0.12 ‰ for $\delta^{18}O(H_2O)$ and ±1 ‰ to ±2 ‰ for $\delta^{2}H(H_2O)$.

We measured the isotopes of dissolved sulfate, $\delta^{34}S(SO_4)$ and $\delta^{18}O(SO_4)$, at IT2E Isotope Tracer Technologies Europe Srl in Milan (Italy). For sulfate, zinc acetate was added to the water samples, and sulfate was precipitated as $BaSO_4$ through the addition of 1 to 2 scoops of $BaCl_2$. We collected and rinsed the precipitate with distilled water until neutrality was reached. The dried samples were weighed into tin cups for separate $^{18}O/^{16}O$ and $^{34}S/^{32}S$ analyses, with a replicate every 3 samples. Approximately 0.1 mg of the sample was used for oxygen analysis. We carried out analysis on a Finnigan Mat, DeltaPlus XL IRMS coupled with a Thermo Scientific TC/EA: samples were pyrolyzed at 1430 °C and purified by gas chromatography before continuous flow isotope ratio mass spectrometry. We corrected and normalized the data via four international standards analyzed at the beginning and end of every run: USGS 32, NBS 127, IAEA SO5, and IAEA SO6, which bracket the samples. The $\delta^{18}O(SO_4)$ values were expressed per mil (‰) relative to V-SMOW. The analytical accuracy for the oxygen analysis was ±0.5 ‰. For sulfur, approximately 0.3 mg of sample was used for $^{34}S/^{32}S$ analysis, with 3 mg of niobium pentoxide added to each sample to ensure complete sample combustion, with 3 samples per replicate. The samples were loaded into a Fisons Instruments Elemental Analyzer for flash combustion at 1100 °C. The released gases were carried by ultrapure helium through the analyzer and then separated by gas chromatography. The cleaned analytical SO_2 gas was carried into a Mat 253 instrument (Thermo Scientific, IRMS) for analysis. The data were corrected and normalized using three international standards analyzed at the beginning and end of every run: IAEA SO6, IAEA SO5, and NBS 127, as well as two calibrated internal standards that bracket the samples. The $\delta^{34}S(SO_4)$ values were expressed in per mil (‰) relative to the Vienna Canyon Diablo Troilite (V-CDT) standards. The analytical precision for analysis was ±0.5 ‰.

We analyzed the strontium isotope ratio and boron isotopic composition (i.e., $^{87}Sr/^{86}Sr$ and $\delta^{11}B$, respectively) at the Department of Geology and Geophysics, University of Utah. For Sr, samples were purified using: 1) 50 ml manual columns with Sr-Spec resin (Eichrom) for Sr/Ca < 0.1 mmol/mol or 2) a 1 ml automatic column with SrCa resin (ESI) in PrepFAST MC for Sr/Ca > 0.1 mmol/mol. Pure Sr fractions were analyzed on a MC–ICP–MS (Neptune; Thermo Fisher Scientific, Waltham, MA, USA) via internal standardization. The Certified Reference Materials used were NIST 987 (strontium carbonate) and USGS EN-1 (carbonate rock). The analytical accuracy was ±0.000006.

For B, the water samples were purified using 50 ml of 1 Amberlite IRA743 resin and 1 ml of sample in an automatic column within PrepFAST MC. Pure B fractions were analyzed on a Neptune MC–ICP–MS via standard bracketing with an in-house B isotopic standard. The following reference materials were used: NIST IAEA B1 (seawater), IAEA B2, and IAEA B3 (groundwater). The $\delta^{11}B$ values were reported in per mil (‰) relative to NIST SRM 951a. The analytical accuracy was ±0.3 ‰.

3.3. Thermodynamic and statistical calculations

We obtained the activity of the dissolved species, saturation indices S.I. = log(IAP/K), where IAP is the ion activity product and K is the equilibrium constant at a specific temperature of a dissolution or hydrolysis reaction and the partial pressure of dissolved carbon dioxide as log$P(CO_2)$ via PHREEQC Interactive software (PHREEQCI, Version 3.7.3; Parkhurst and Appelo, 2013) using the llnl.dat and Thermoddem (Blanc et al., 2012) thermodynamic databases and Geochemist's Workbench® software (GWB, Release 12.0.9; Bethke et al., 2022) via the Thermo.tdat database. In particular, the Thermoddem database was integrated with the solubility data of leucite (Holland and Powell, 2011), pollucite (Ogorodova et al., 2003), and muscovite (disordered) (Blanc P., personal communication), which were calculated according to Boschetti et al. (2024) (Supplementary Material 1). Moreover, we used NetPathXL code (Version 1.5.1; Parkhurst and Charlton, 2008) to compute the mixing proportions of two to five initial waters and net geochemical reactions that can account for the observed composition of the final water.

Principal component analysis (PCA) is a statistical tool that can discover unsuspected relationships that can reduce the dimensionality of a dataset while retaining the information present in the data structure. It has been successfully applied to explain the hydrogeochemical composition of thermal waters in different geological settings (e.g., Nicholson, 1993; Boschetti et al., 2003; Awaleh et al., 2020; Barbieri et al., 2021). In this study, OriginPro Version 2023 (OriginLab Corporation, Northampton, MA, USA) was used to extract the independent principal components from the correlation matrix constructed on the basis of the physico-chemical composition of the sampled springs. Moreover, using the same software and data matrix, we calculated a correlation plot at a significance level of 0.05 (see Supplementary Material 2).

4. Results

4.1. Structural survey

In this section, we summarize from north to south the new field observations along the fault bordering the piedmont of the Pontina Plain. As illustrated in Fig. 3, in conjunction with the hydrogeologic map of the springs in Fig. 2d, the alignments correspond to 10 km long segments of an oblique normal fault exhibiting varying flat topographic expressions at their footwall, ranging from approximately 400 m above sea level in the north (Fig. 3a-c) to approximately 600 m in the south (Fig. 3d).

These variations are associated with structural and morphologic characteristics marked by the coexistence of transtensive high-angle faults (Fig. 3e-f) and an uplifted subhorizontal to tilted plateau located at the footwall of a normal fault system, where kinematic indicators reveal a significant strike–slip component. The fault zone crops out within the carbonate formations of cliffs between Norma and Ninfa springs (Fig. 3b-c), at the Monticchio quarry (Fig. 3d-e), and near the sulfur-rich springs at the La Catena locality. While the oldest exposed carbonates in the north are Jurassic (Fig. 3b-c), the footwall in the south comprises Cretaceous group units (Fig. 3d). Joint and fracture systems within the fault zone are locally filled with travertine and alabaster concretions, indicative of past fluid circulation. On the plain, the carbonate hanging wall is overlain by a Quaternary succession reaching minimal thicknesses of approximately 100 m near the escarpment (Serva and Brunamonte, 2007) (Section 5.1). Sedimentary red breccias, typically related to the Late Pleistocene (older than 35 Ka; Alessandri et al., 2021 and references therein), cover the fault zone and are intersected by a series of faint joints and faults with poorly defined slickenlines.

In the southern region (Fig. 4), the footwall plateau and the slope adjacent to the Pontina Plain border fault are both punctuated by several dolines, while the plain features numerous sinkholes, some of which harbor sulfur-rich hypothermal springs (Fig. 4a-b) (see Section 5.2). The footwall plateau in this area sits at approximately 150–200 m above sea level, whereas the top of the hanging wall carbonates lies at greater depths (see Section 5.1). The fault zone is exposed near one of the sampled Laghi del Vescovo and Fontana di Muro spring localities (Fig. 4c-e) and consists of a fault core several meters thick flanked by a damaged carbonate zone. Similar to observations in the northern region, field evidence indicates that joints traversing the Upper Pleistocene breccia align with faults that are organized into synthetic and antithetic

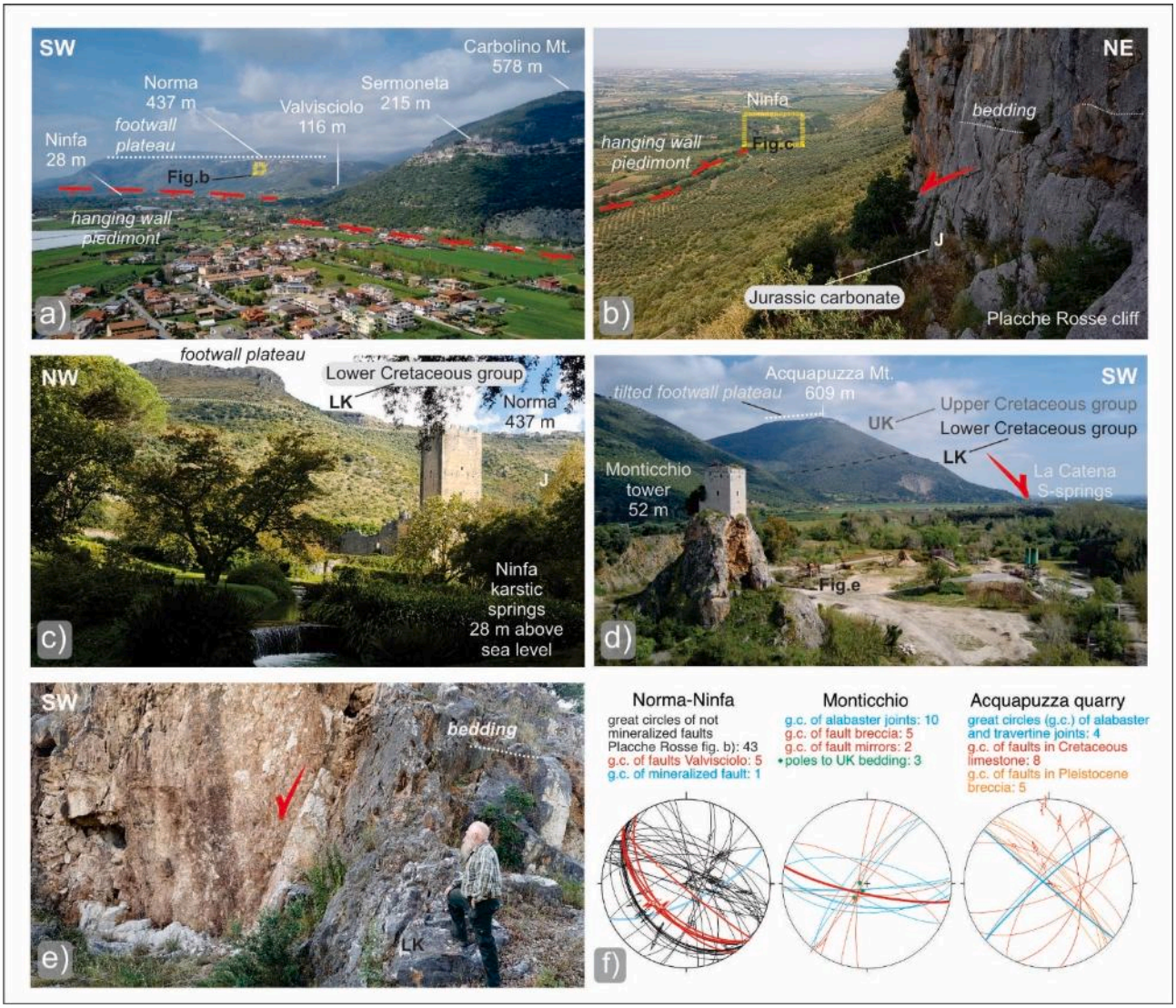

Fig. 3. Structural features along the fault bordering the Lepini Mounts, depicted from north to south. The segments of the fault align with topographic variations (uplifted and tilted plateau), ranging from approximately 400 m above sea level in the north (a-c) to approximately 600 m in the south (d). Transtensive high-angle faults at the footwall exhibit a strike-slip component in the stereoplots (lower hemisphere projection, equal area) (e-f).

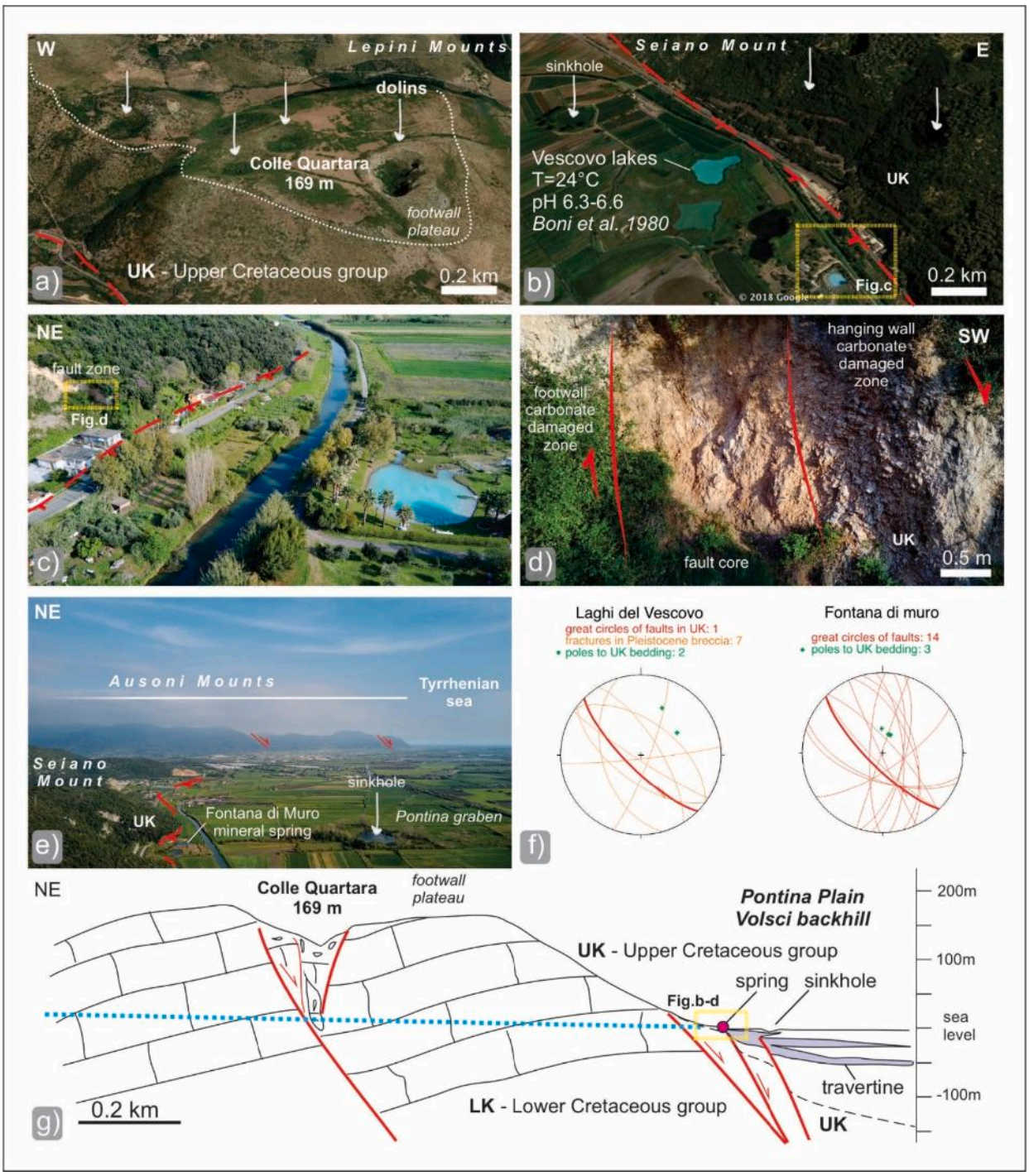

Fig. 4. Geomorphological and hydrogeological characteristics in the southern zone adjacent to the Pontina Plain border fault. Dolines punctuate the footwall plateau and slope, whereas sinkholes, some hosting sulfur-rich hypothermal sources, are prevalent on the plain (a-b). The fault zone, characterized by a fault core and damaged carbonate zone, is exposed near Laghi del Vescovo and Fontana di Muro (c-e). Structural elements of the sampled localities highlight the variability of fractures within Upper Pleistocene breccia with respect to the main faults (red great circles in the stereoplots, lower hemisphere projection, equal area) (f). Schematic geologic cross-section showing how karstic forms are closely related to faults and the piezometric level from Celico (1980) (g).

systems (Fig. 4f). As depicted in Fig. 4g, karstic formations are closely associated with faults and piezometric levels. Supported by field evidence near the spring and the presence of travertine in the initial 50 m of the post-Tyrrhenian alluvial succession, mineralized waters have characterized the piedmont region of the Pontina graben since at least the Late Pleistocene.

4.2. Hydrogeochemical characterization

We present the chemical–physical parameters and hydrogeochemical compositions (i.e., major ions and trace elements) of the sampled groundwater in Table 1 and Supplementary Material 3. The electrical conductivity (EC) provides good preliminary hydrogeochemical information for characterizing the springs. According to the measured EC values, three groups of springs can be distinguished.

The first group (1, springs: PR, PS, N, NB, C, and AZ) presented values ranging from 421 to 805 μS/cm; the second group (2, springs: AP and FM) presented values ranging from 1088 to 1241 μS/cm; and the third group (3, springs: PC and GV) presented values ranging from 2100 to 4800 μS/cm. This first observation indicates that the investigated springs are characterized by different degrees of mineralization. To better understand this feature, we also calculated the TDS (total dissolved solids) of the springs as the sum of the concentrations (in mg/l) of the primary dissolved constituents (Baird et al., 2017; Boschetti et al., 2019; Table 1). The minimum and maximum values of TDS are 225 mg/l and 2977 mg/l for N (Group 1) and GV (Group 3), respectively.

According to the Schoeller classification (Schoeller, 1962), by considering the mean annual air temperature of the study area, which is approximately 16.5 °C (https://it.climate-data.org), most water samples are hypothermal ($T_{spring} < T_{air}$), whereas GV waters are orthothermal ($T_{air} < T_{spring} < T_{air} + 4$ °C), with temperatures ranging between 18.40 °C and 19.10 °C. However, in previous studies (e.g., Deffenu et al., 1975), temperatures up to 23 °C were detected in the springs of the GV area; therefore, these temperatures could be classified as orthothermal to thermal ($T_{spring} > T_{air} + 4$ °C), implying a deeper flowpath related to the fault system.

The Langelier–Ludwig diagram was constructed to identify which major ions are predominant in the abovementioned groups (Fig. 5). All the springs in Group 1 cluster in the low-right corner and are enriched mainly in bicarbonate and calcium ions, thus showing Ca–HCO_3 facies and substantial compositional homogeneity (Fig. 5). The springs of Group 2 are characterized by a clear enrichment of chloride, resulting in intermediate Ca–SO_4(Cl) facies. Finally, following a linear trend of hydrogeochemical mixing toward the Na–Cl water domain, a high alkali content is noted for the springs of Group 3. The most mineralized Na–Cl springs (i.e., GV and PC) are depicted as triangles and fall near the F-field, representing the water samples from the borehole drilled at Fogliano (Latina, Fig. 2) (Boni et al., 1980; Camponeschi and Nolasco, 1983; Schettino, 1999). As shown in Fig. 5, the global data trend of this study is in line with those previously published (depicted as smaller white circles) carried out on the Pontina Plain (Deffenu et al., 1975; Boni

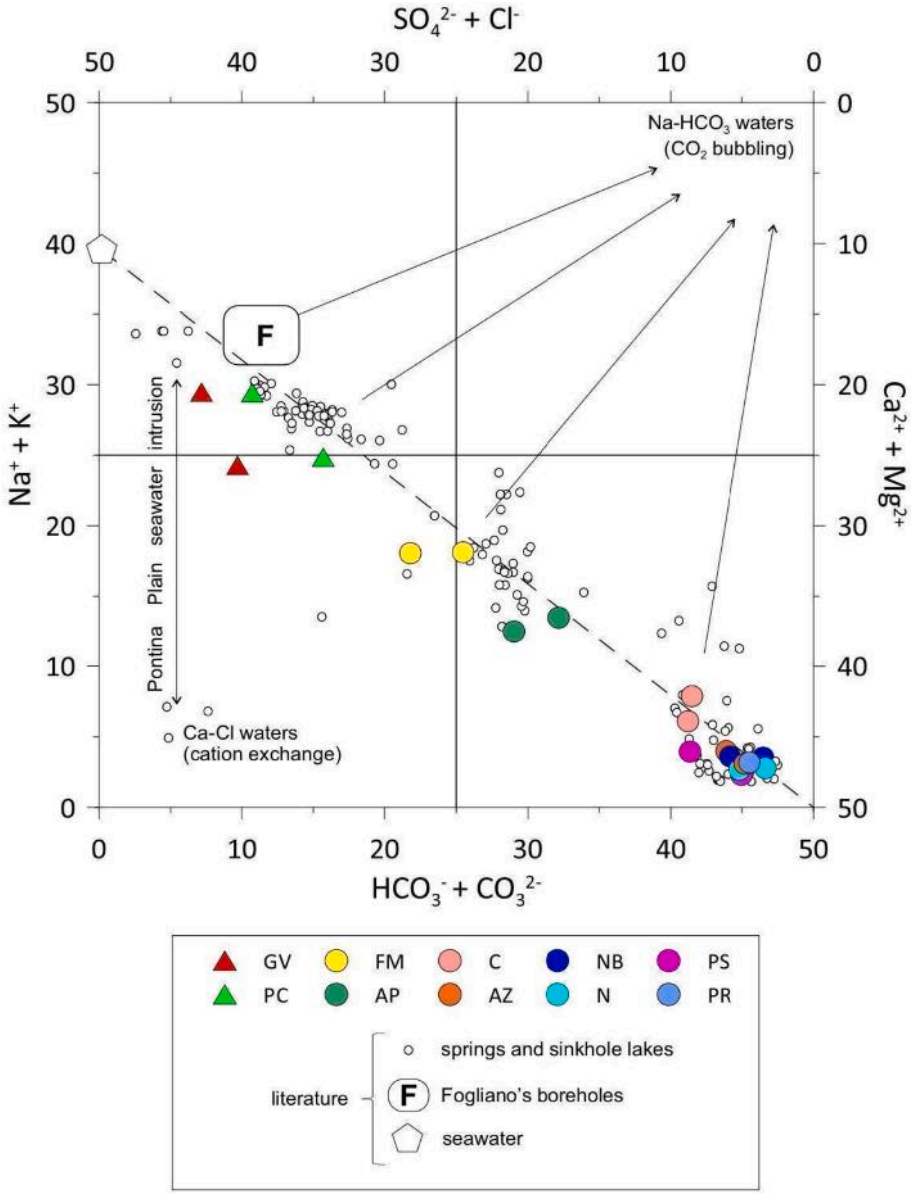

Fig. 5. Langelier–Ludwig diagram for all the collected samples (equivalent basis concentrations). The colored symbols are data from this study, and the white symbols (both small circles, F-fields, and seawater pentagons) are from the literature (see the main text for the reference list). For the spring IDs, refer to Table 1 and Fig. 2d-e, where the location is outlined. Dashed line: hypothetical meteoric–seawater binary mixing.

et al., 1980; Giggenbach et al., 1988; Governa et al., 1989; Duchi et al., 1991; Tuccimei et al., 2005; Sappa et al., 2012).

The shallow karstic groundwater from the northern VR and the direct involvement of seawater in determining the trend from Ca–HCO_3 toward Na–Cl facies were hypothesized by Bono (2011), who also suggested the presence of a deep hydrothermal system from the crystalline basement. The presumed local marine ingression was confirmed in the southern sector of the Pontina Plain near the Tyrrhenian Sea (Sappa and Coviello, 2012). There, variable water compositions ranging from Na–Cl to Ca–Cl due to seawater intrusion followed by Na–Ca cation exchange were found (Fig. 5; e.g., Appelo and Postma, 2004). Boni et al. (1980) and Governa et al. (1989) hypothesized the possible contribution of deep fluids similar to those from the Fogliano boreholes, speculating on the interaction between carbonate successions containing evaporites and acidic fluids upwelling through the crust. Following this interpretation, Boni et al. (1980) stated that "the temperature of the deep hydrothermal circuit, estimated using geothermometers, was found to be 180–200 °C for the Fogliano borehole and 180 °C for the Laghi del Vescovo" (Figs. 2, 4). These geothermometric estimates, which are based on the albite–K–feldspar (Na–K) equilibrium and the empirical Na–K–Ca geothermometer (Boni et al., 1980), should be reviewed. Additionally, the validity of water–mineral equilibria should be tested with appropriate activity diagrams by considering potential interactions with sulfates and zeolites, which could affect the results of equilibria based solely on Ca^{2+} from silicates, as in the empirical Na–K–Ca geothermometer (Cioni and Marini, 2020).

Finally, the presence of deep CO_2 and cold interactions at very shallow depths with magmatic products has also been suggested (Boni et al., 1980; Duchi et al., 1991; Nisio, 2008; Bono, 2011). Specifically, some water samples with predominantly alkaline–bicarbonate compositions resulting from the latter process were detected by Bono (2011). Unfortunately, the exact location of these samples is unknown. However, some secondary trends that deviate from the global trend toward the Na(K)–HCO_3 composition could support the hypothesis of diffuse CO_2 input in the area (Fig. 5). All these processes can simultaneously constitute a Na–Cl hydrogeochemical facies for the most mineralized waters on the Pontina Plain, increasing the abundance of chloride ions.

Additionally, principal component analysis (PCA) was applied to major ions and trace elements to identify groupings or clusters of samples on the basis of compositional similarities (Holmslykke et al., 2019). The PCA results are presented as a biplot (Fig. 6) showing both the component scores of the samples (red dots) and the loadings of the variables (eigenvectors displayed in blue). The PCA results show different groups of samples and variables: the GV samples present positive values of PC1 and PC2, which correlate with Ga, Na, Cl, Cs, Rb, EC, Li, B, SO_4, Mg, T, Co, K, and Sr. Similarly, the samples from the PC spring had positive score values on PC1 but lower values (close to zero) on PC2. Therefore, PC samples seem to be principally correlated with the last four variables listed above, together with Ca. The clustering of these two springs (i.e., GV and PC) could be ascribed to their greater temperature and salinity. Indeed, they were the only two brackish samples (TDS > 1 g/l) detected in this study. However, the primary anomaly of the GV samples remains to be explained, particularly for the trace elements Ga, Li, Rb, Cs, and B, which may indicate interactions with magmatic rocks (see Sections 5.2–5.3). The samples from the AP spring had positive values for PC1 and negative values for PC2, which were related mainly to HCO_3, Fe, and Mn. In the opposite quadrant, where the PC2 values were positive and the PC1 values were negative, the samples from the springs close to Ninfa Lake (N and NB) are grouped (Fig. 6). Despite their lowest salinity (0.2 g/l) and sulfate concentration (~5 mg/l), these springs present anomalous concentrations of Cr, V, Mo, and Al and pH values that were higher than those of other springs. This variable cluster could be associated with the decomposition of organic matter (e.g., Smedley and Kinniburgh, 2017), as evidenced by the constant presence of dissolved nitrates. Finally, the remaining springs with intermediate salinities (0.4–0.8 g/l) formed a cluster with negative values for both PC1 and PC2.

In the correlation plot (Supplementary Material 2), the positive and

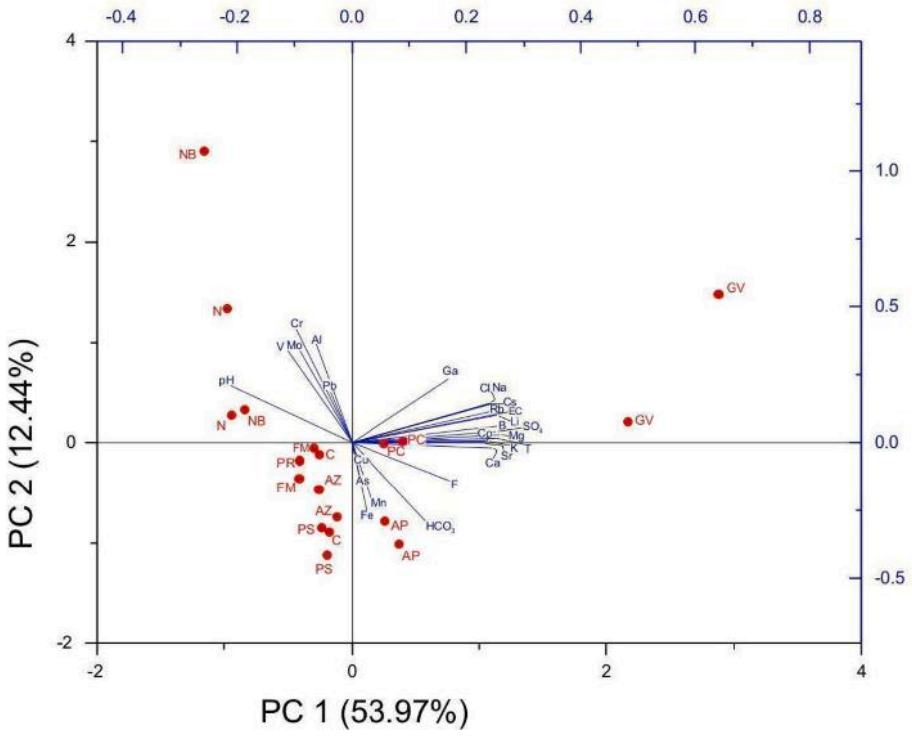

Fig. 6. Principal component analysis (PCA) plot. Both the loadings of the variables (eigenvectors, in blue) and the component scores assigned to the samples (red dots with the ID of the spring samples) are shown in relation to the first two components (PC1 and PC2). Preliminary data (e.g., correlation matrix) and full results of the PCA are provided in Supplementary Material 4.

significant correlations mainly concern the relationships between the main constituents and the chemical–physical variables. Among these, the highest and most significant Pearson correlation coefficients (r) pertain to the relationships between Na–Cl (1.0); EC–Na and EC–Cl (0.99); Mg–SO_4 (0.98); T–SO_4 and EC–Mg (0.97); Cl–SO_4, EC–SO_4, and T–EC (0.96); and K–SO_4, Mg–Cl, and Na–SO_4 (0.95). This is primarily because at relatively high salinity (and EC) levels, the Na and Cl variables dominate, whereas the sulfate and magnesium concentrations, resulting from the dissolution of gypsum/anhydrite and dolomite, respectively, are subordinate and at lower concentrations. Exceptions include carbonate alkalinity (cAlk = HCO_3), which mainly had nonsignificant correlations (except for Ca–HCO_3 with $r = 0.63$ according to carbonate dissolution and scattered values at lower concentrations), and pH, which mainly shows inverse (negative r) relationships. For most trace elements, we also observed nonsignificant correlations, except for the r values of Li–B (0.99), Li–Cs (0.98), and Li–Rb (0.97). The results of multiple isotopes of $\delta^{18}O(H_2O)$, $\delta^{2}H(H_2O)$, $\delta^{34}S(SO_4)$, $\delta^{18}O(SO_4)$, $^{87}Sr/^{86}Sr$, and $\delta^{11}B$ are listed in Table 2. Stable isotopes of water $\delta^{18}O(H_2O)$ and $\delta^{2}H(H_2O)$, measured for five selected groundwater samples (i.e., N, AP, AZ, PC, and GV), ranged from −7.3 to −6.6 ‰ and between −43 and −39 ‰, respectively. The $\delta^{34}S(SO_4)$, $\delta^{18}O(SO_4)$, $^{87}Sr/^{86}Sr$, and $\delta^{11}B$ values were analyzed only for the springs included in Groups 2 and 3 (see Table 2).

5. Discussion

In this section, we discuss the structural geometry of the study area and the fluid circulation within a fault–controlled karstic setting. Our objective is to constrain a conceptual groundwater flow model supported by a hydrogeochemical multicomponent approach. We also discuss the different aspects of the groundwater signature to identify the sites and processes of both mixing and water–rock interactions in a major fault zone.

5.1. Structure of the Pontina Plain and the adjoining karstic aquifer

As depicted in Fig. 7a, we reconstructed the deep structure of the Pontina Plain and the adjoining karstic aquifer of the VR, considering the available public data of the studied region. In light of the new structural data presented in Figs. 3 and 4, the fault edging the Pontina Plain has a stepwise shape of segments that are as long as 10 km. These segments are associated with a minimum displacement of 500–600 m near Norma and approximately 600–700 m at La Catena, where S-rich springs are likely related to the intersection with the main NW-striking main fault intersecting the outcropping Upper Pleistocene breccia. Considering that faults with similar surface rupture lengths occur in the Ausoni Mounts (Alessandri et al., 2021), reach up to 10–12 km, and have structural offsets on the order of 0.8–1 km, we estimate that the morphostructural elevation of the plateau reported in Figs. 3 and 4 for the fault edging the Pontina Plain accounts for only a part of the actual structural offset across the fault, thus lining up with the 0.8–1 km described above. Faults and fractures associated with the studied fault zone became sites of travertine precipitation (Fig. 3). In these areas, the presence of alabaster and speleothem concretions aligned with minor NE-striking faults highlights the presence of long-lasting circulation of fluids within minor cross-faults. Furthermore, the presence of dolins overprinting the fault-related morphostructures of the fault edging the Pontina Plain and the presence of active sinkhole formation on the plain (Bono, 1995; Figs. 3 and 4) suggest ongoing morphostructural evolution related to fluid circulation. To establish a larger-scale structural model that allows us to determine the deep structure of the southern sector, where mineralized waters occur, we used information from available wells and seismic lines (Cardello et al., 2020, 2021).

To reconstruct the subsurface geometry, we used two main key horizons: the bottom of the Plio–Pleistocene *syn*-rift units (MVA) and the top of the Triassic units, identified by the wells in Fig. 6b. Triassic evaporitic layers (*Anidriti di Burano* Formation, BU, Fig. 7b) were found at approximately 2100 m depth in the Latina Gulf, with a thickness of approximately 450 m. The other Triassic units are dolostones. They occur offshore and onshore of the southern VR, with minimum stratigraphic thicknesses of approximately 650 and 1800 m, respectively. Extensive outcrops near Gaeta reach a minimal stratigraphic thickness of approximately 200–250 m (Fig. 7a). Fig. 7c-d presents the reinterpretation of a crucial seismic line, aiming to identify sites of groundwater interaction with various rock types at depth, including evaporitic formations, which mix with the dominant karstic freshwater component. The reinterpretation of seismic line LT-328-86 V in Fig. 7c-d provides insights into the tectonic setting at depth. In line with previous interpretations (Milia and Torrente, 2015; Milia et al., 2017; Tavani et al., 2023), our model aims to delineate in greater detail the Quaternary normal faults within the Pontina Plain. We constrain the top of the carbonate substrate from the near-surface to approximately 0.2–0.3 s

Table 2
Isotopic contents of springs from the study area are reported (sample ID corresponds to the sites displayed in Fig. 2d-e).

Sample ID	Sampling date	$\delta^{2}H(H_2O)$	$\delta^{18}O(H_2O)$	$\delta^{18}O(SO_4)$	$\delta^{34}S(SO_4)$	$^{87}Sr/^{86}Sr$	$\delta^{11}B$
	(dd/mm/yyyy)	V-SMOW	V-SMOW	V-SMOW	V-CDT	NIST 987	SRM 951a
GV	30/01/2020	−39	−6.6	–	–	–	–
GV	19/10/2020	–	–	–	–	–	–
GV	12/02/2021	–	–	13.4	21.4	0.707942	13.83
C	30/01/2020	–	–	–	–	–	–
C	19/10/2020	–	–	–	–	–	–
AZ	30/01/2020	−42	−7.1	–	–	–	–
AZ	19/10/2020	–	–	–	–	–	–
PC	30/01/2020	−40	−6.9	–	–	–	–
PC	19/10/2020	–	–	–	–	–	–
PC	12/02/2021	–	–	9.6	15.8	0.708172	18.45
NB	30/01/2020	–	–	–	–	–	–
NB	19/10/2020	–	–	–	–	–	–
N	30/01/2020	−43	−7.3	–	–	–	–
N	19/10/2020	–	–	–	–	–	–
FM	30/01/2020	–	–	–	–	–	–
FM	19/10/2020	–	–	–	–	–	–
FM	12/02/2021	–	–	9.2	13.9	0.707873	20.75
AP	30/01/2020	−41	−7.0	–	–	–	–
AP	12/02/2021	–	–	9.5	14	0.708061	7.39
PS	30/01/2020	–	–	–	–	–	–
PS	19/10/2020	–	–	–	–	–	–
PR	30/01/2020	–	–	–	–	–	–

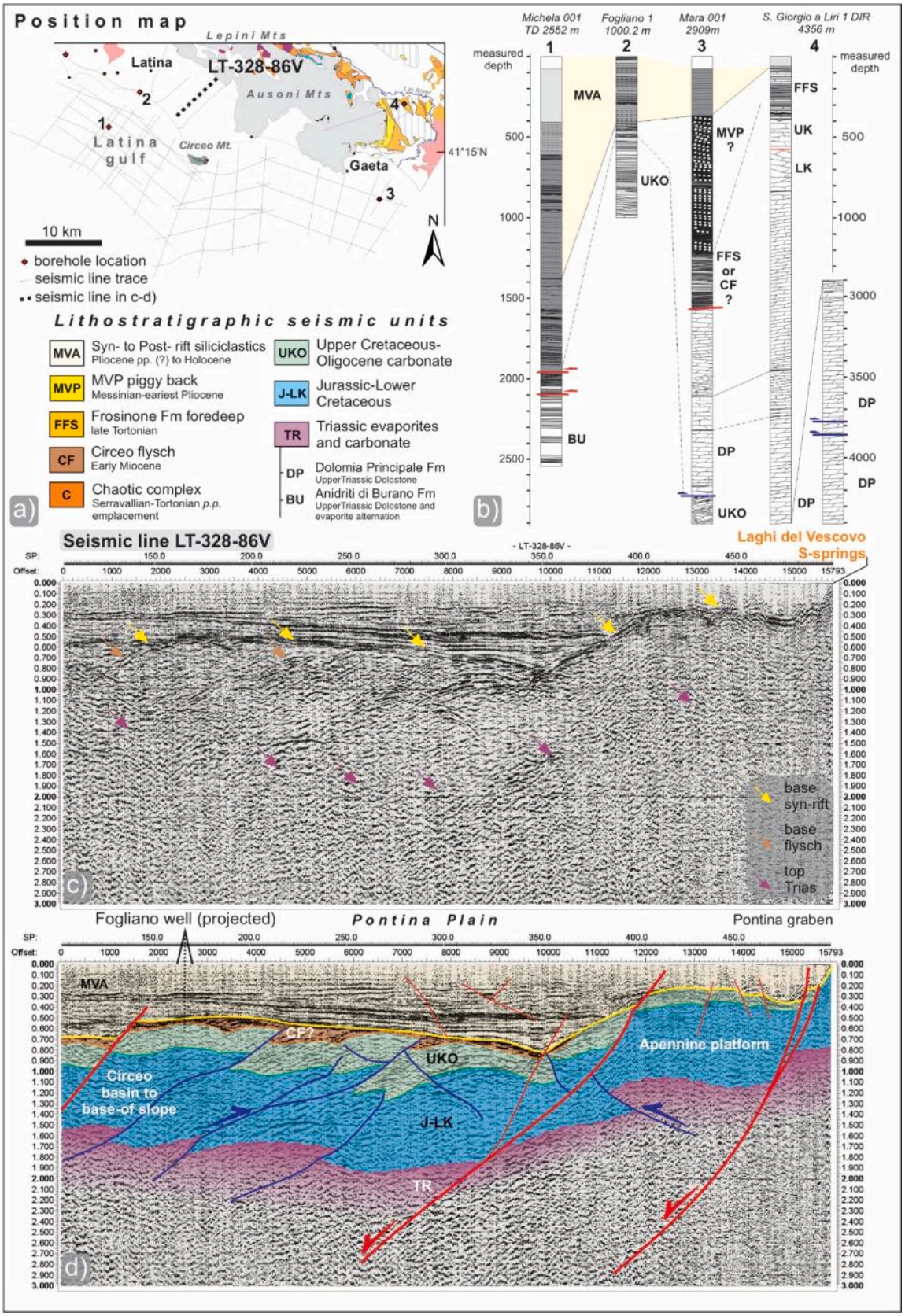

Fig. 7. Subsurface insights into the Pontina Plain aimed at establishing a structural framework for groundwater interaction with Triassic rock types at depth. (a) Position map indicating the distribution of public subsurface data for southern Latium onshore and offshore (modified from Cardello et al., 2021). (b) Comparison of lithostratigraphic data from wells on the Pontina Plain and southern VR, highlighting the presence of a Triassic evaporitic unit (BU). (c-d) Two-way travel (TWT) seismic lines (from www.videpi.com; accessed on 10 April 2024), with interpretations, also depicting the projection of the Fogliano borehole.

near the Pontina graben, 0.8 s in the depocenter of the plain, and 0.5 s near the southwest coast. The maximum thickness of the siliciclastic succession corresponds to approximately 0.5 km at the Fogliano borehole to approximately 1.5 km in the middle of the Pontina Plain, while it is much thinner near the VR (approximately 0.3–0.5 km thick). Geometric relationships and Quaternary geomorphic evidence indicate that normal faults overlay the inherited Miocene fold-and-thrust system, highlighted by the top-Triassic reflector depth of approximately 2.5–3 km at the hanging wall of the fault edging the VR, creating a horst and graben structure tied to the Tyrrhenian margin back-arc extension and its thermal anomaly (https://geothopica.igg.cnr.it). Overall, our interpretation suggests that carbonate units host an unconfined aquifer and semiconfined aquifers to a limited extent, characterized by variable salinity and hydrogeochemistry depending on the heterogeneity of lithological types (Tuccimei et al., 2005).

5.2. Stable isotopes of water (δ^2H and $\delta^{18}O$)

The isotopic compositions of the water molecules in the samples analyzed in this study highlight their meteoric origin, which is in line with previously published results (Boni et al., 1980; Governa et al., 1989; Duchi et al., 1991). In particular, all spring waters fall within (Fig. 8): i) the global meteoric water line (GMWL; Gourcy et al., 2005), which has a deuterium excess d = 10.9, and the line of the spring waters from carbonate aquifers in Central Italy d = 17 (Celico et al., 1984; Governa et al., 1989) (Fig. 8); and ii) the confidence interval (C.I.) calculated on mean data of the weighted-amount precipitation at five weather stations in the Latium region (Fiori, 2007): $\delta^2H(H_2O) = 7.01$ ($\pm$0.42) $\times$ $\delta^{18}O(H_2O)$ + 6.7($\pm$2.4). However, contrary to the findings in the literature, the samples show a clearer alignment toward the composition of the water from the borehole at Fogliano, with $\delta^{18}O(H_2O) = -6.2$ ‰ and $\delta^2H(H_2O) = -35$ ‰ (F-field in Fig. 8) (Boni et al., 1980; Governa et al., 1989), rather than toward seawater, with $\delta^{18}O(H_2O) = \delta^2H(H_2O) = 0$ ‰. In particular, the GV sample has the most significant contribution from deep fluid (Fig. 8). Furthermore, samples indicate a predominant recharge from the northern VR (Fig. 2), falling within the C.I. of the meteoric line of the area, $\delta^2H(H_2O) = 4.01(\pm0.47) \times \delta^{18}O(H_2O)$ - 13.0($\pm$3.0) (data from Sappa et al., 2012) (Lepini Mount meteoric water line in Fig. 8). The large scatter of literature data around that line is probably due to greater analytical uncertainty. In contrast, the more positive oxygen and hydrogen ratios of the Fogliano borehole water (F-field in Fig. 8) in the confidence interval of the Latium meteoric water line are probably due to a recharge contribution from the coastal area, which is consistent with the isotopic data from the Fogliano meteorological station (5 m a.s.l.): $\delta^{18}O(H_2O) = -4.34$ ‰ and $\delta^2H(H_2O) = -20.3$ ‰ (Fiori, 2007). Finally, both the water from the Fogliano borehole and the sampled springs show a mean deuterium excess of d = 14.6, which is very close to the value of d = 15 inferred for the Tyrrhenian/Central Mediterranean area (Gat and Carmi, 1970).

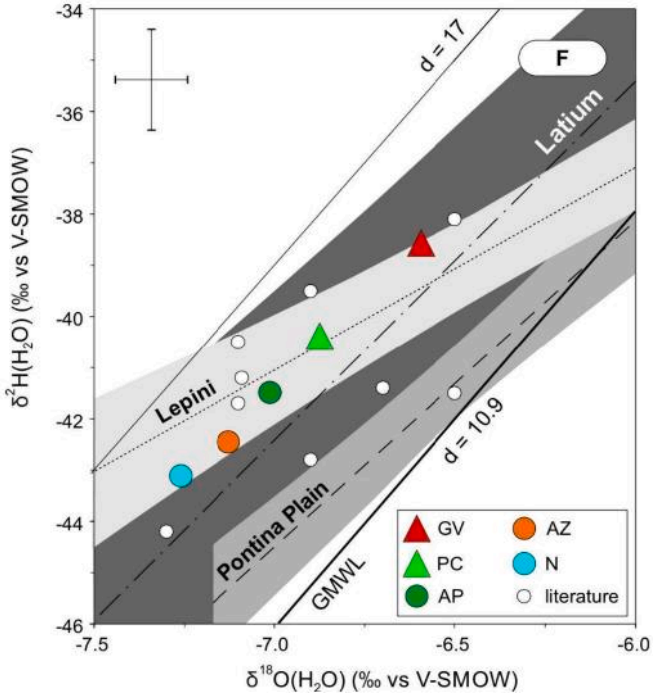

Fig. 8. Oxygen and hydrogen stable water isotope ratios, in ‰, versus V-SMOW (this study) or SMOW (literature). Thick and thin continuous lines depict the composition of precipitation at the global scale (Gourcy et al., 2005) and that from carbonate aquifers in Central Italy (Celico et al., 1984), with deuterium excesses of d = 10.9 and d = 17, respectively. The dotted–dashed line with the dark gray confidence interval (C.I.), the dotted line with the light gray C.I., and the dashed line with the gray C.I. are the meteoric lines of Latium (Fiori, 2007), the Lepini Mounts, and the Pontina Plain (Sappa et al., 2012), respectively. Literature data, including Fogliano borehole water (F-field), are also shown for comparison (Boni et al., 1980; Governa et al., 1989; Duchi et al., 1991). The abbreviations of the springs are listed in Table 1.

5.3. Isotope ratios of dissolved strontium ($^{87}Sr/^{86}Sr$), sulfate ($\delta^{34}S$ and $\delta^{18}O$) and boron ($\delta^{11}B$)

Using the individual analyses of the isotope ratios of dissolved strontium ($^{87}Sr/^{86}Sr$), sulfate ($\delta^{34}S$ and $\delta^{18}O$), and boron ($\delta^{11}B$), we aim to discern the types of rocks that groundwater has encountered and determine whether multiple fluid–rock interactions can be distinguished at the edging fault of the Pontina Plain, along with the temperatures at which these interactions occurred. The isotope ratios of dissolved strontium and sulfate can provide valuable insights into water–rock interaction processes. With respect to strontium, the $^{87}Sr/^{86}Sr$ ratios of the spring water samples in this study ranged between 0.7079 (GV) and 0.7081 (AP). Specifically, the lower value of GV is compatible with a predominant contribution from Upper Triassic evaporites. Globally, this period has values ranging from 0.7077 (late Rhaetian, 201.46 Ma) to 0.7080 (late Norian, 210.2 Ma) (McArthur et al., 2020), and the central value of this range coincides with the average value of gypsum/anhydrite samples from the *Anidriti di Burano* Formation from the same period (0.7078 $\pm$ 0.0001, $N = 7$; Boschetti et al., 2017). The comparison with other literature data as a function of the reciprocal concentration of Sr (Fig. 9) does not reveal appreciable and diagnostic shifts toward carbonate or volcanic rocks. Presumably, this is due to the higher solubility of sulfate minerals and their high strontium concentration (Boschetti et al., 2005).

This hypothesis is also supported by the dissolved sulfate isotopic composition diagram (Fig. 10a), where water samples are close to the primary samples, with $\delta^{34}S(SO_4) = 15.5 \pm 0.4$ ‰ and $\delta^{18}O(SO_4) = 10.8 \pm 1.2$ ‰ (99 % C.I.; Boschetti et al., 2011), and secondary (i.e., alteration by *syn*- or postdepositional processes) gypsum and anhydrite from the Upper Triassic *Anidriti di Burano Formation* in the northern Apennines (Boschetti et al., 2011), which was also encountered offshore of the Pontina Plain in the Michela 1 well (Figs. 2, 7b). Additionally, based on a comparison of the literature data from the northern VR and springs with the primary *Anidriti di Burano* Formation composition, as highlighted in Fig. 10a, a substantial enrichment in the GV sample (Governa et al., 1989) occurs, while a depletion occurs in the other samples. The observed divergent trends are likely attributable to an intermediate kinetic bacterial reduction process, resulting in an enrichment of residual sulfate, and a process involving the oxidation of dissolved sulfide in shallower (and oxidized) waters (Fig. 10b). Considering the overestimation of approximately 1 ‰ of the $\delta^{18}O(SO_4)$ values in the literature data (Boschetti, 2013; Boschetti and Iacumin, 2005), it is possible to calculate a temperature of approximately 98 °C for the Fogliano borehole via the $10^3 ln\alpha^{18}O_{(anhydrite\text{-}water)}$ fractionation factor (Boschetti

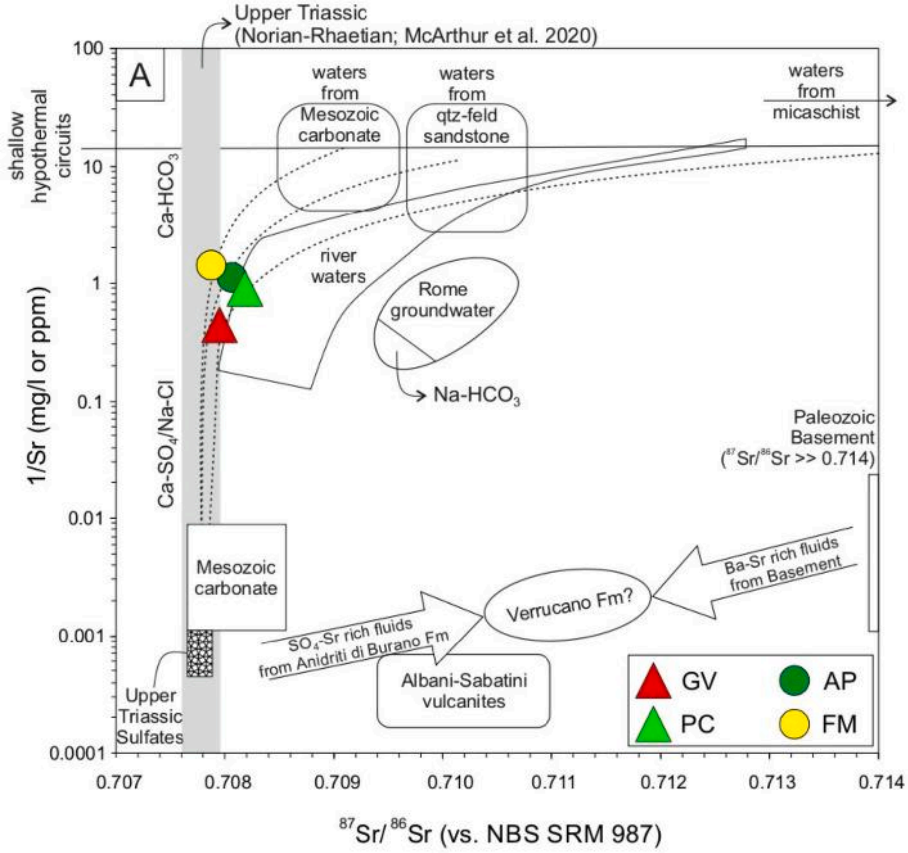

Fig. 9. 1/Sr (mg/l for water or ppm for rocks and minerals) versus the $^{87}Sr/^{86}Sr$ ratio, modified from Boschetti et al. (2017). Compared with the latter, Rome groundwater and Albani/Sabatini volcanoes (Barbieri et al., 1975; Pizzino, 2015) were added. The "Upper Triassic sulfate" hatched field encloses the values of gypsum and anhydrite in the Apennines (*Anidriti di Burano* Formation; Boschetti et al., 2017). The dotted curves are binary mixing paths. The abbreviations of the springs are listed in Table 1.

et al., 2011). The obtained value is compatible with an estimate of 93 °C via the Na–Li geothermometer for waters from sedimentary basins (Eq. (9) in Sanjuan et al., 2014) and the chemical data from the Fogliano borehole (Camponeschi and Nolasco, 1983). Furthermore, taking into account the geothermal gradient map of the study area (Trumpy and Manzella, 2017), the depth corresponding to the average temperature of 95.5 ± 3.5 °C is estimated to be approximately 3 km, which, according to the interpreted seismic line in Fig. 6c-d, could lie within Triassic units that are likely to be connected with the evaporitic buried succession drilled in the Gulf of Latina (Michela 1 well, Figs. 2, 7b).

By analyzing boron isotopes, we assume that the dissolved boron in the sampled springs has a geogenic origin. In fact, to the best of our knowledge, there has been no evidence of anthropogenic boron pollution in the groundwater of the study area. Indeed, the boron concentration is well below the 2.4 mg/l guideline value (WHO, 2022). Furthermore, as all springs swing around neutrality with negligible fluctuations, fractionation due to pH can be ruled out. Nevertheless, in contrast to strontium and sulfate, the isotopic stratigraphy capability for the $^{11}B/^{10}B$ isotope ratio has yet to be discovered. This implies that the age of the marine carbonate–evaporitic formation, with which groundwater has interacted, cannot be determined. This limitation also affects palaeoceanographic studies, which remain largely empirical (Branson, 2018). Despite this, boron dissolved in four selected springs (two Na–Cl springs, GV and PC, and the two "intermediate" compositions, AP and FM) seems to be determined by multiple natural sources that, in the first approximation, could be related to carbonates and silicates, in addition to the already mentioned evaporites (Fig. 11). While the sedimentary lithologies are likely intersected by the fault edging the Pontina Plain, magmatic rocks are not known to exist at depth, although their role was already envisaged by Boni et al. (1980). Therefore, as best depicted later in Section 5.4, it is worth noting that most major faults in the northern VR were utilized by monogenetic magmatism during the Pleistocene (Cardello et al., 2020; Marra et al., 2021). In our particular case, we highlight that GV is characterized by the most significant thermal anomaly, which falls close to the intersection of two binary mixing curves, namely, i) boron from interactions with carbonates and release from volcanic units at high T (> 25 °C) and ii) boron from Upper Triassic evaporites and release from clay minerals (Boschetti et al., 2019). Therefore, the boron isotopic composition appears to be regulated by complex four-member mixing.

5.4. Interpretative hydrogeological model

In this section, we discuss the plausibility of our findings in terms of the sites of mixing and the groundwater–rock interaction processes. According to the analyses conducted in our study area, the hydrogeochemical composition of springs along the piedmont transtensive fault edging the Pontina Plain exhibited a progressive increase in mineralization (Figs. 2, 3) toward the southeast (Figs. 2, 4). Thus, some water–rock equilibria were examined through activity diagrams, saturation indices, CO_2 partial pressures, and abundances of several specific trace elements (e.g., Li–Rb–Cs).

In the Na^+/H^+ vs. K^+/H^+ activity diagram (Supplementary Material 5), a large portion of the water samples lies within the stability field of kaolinite. The only exception is represented by GV, which shows enrichment in the K^+/H^+ ratio, likely due to mixing with fluid from the Fogliano borehole, recalculated at a temperature of 95 °C (F-field) obtained in Section 5.3. Owing to the thermodynamic and compositional

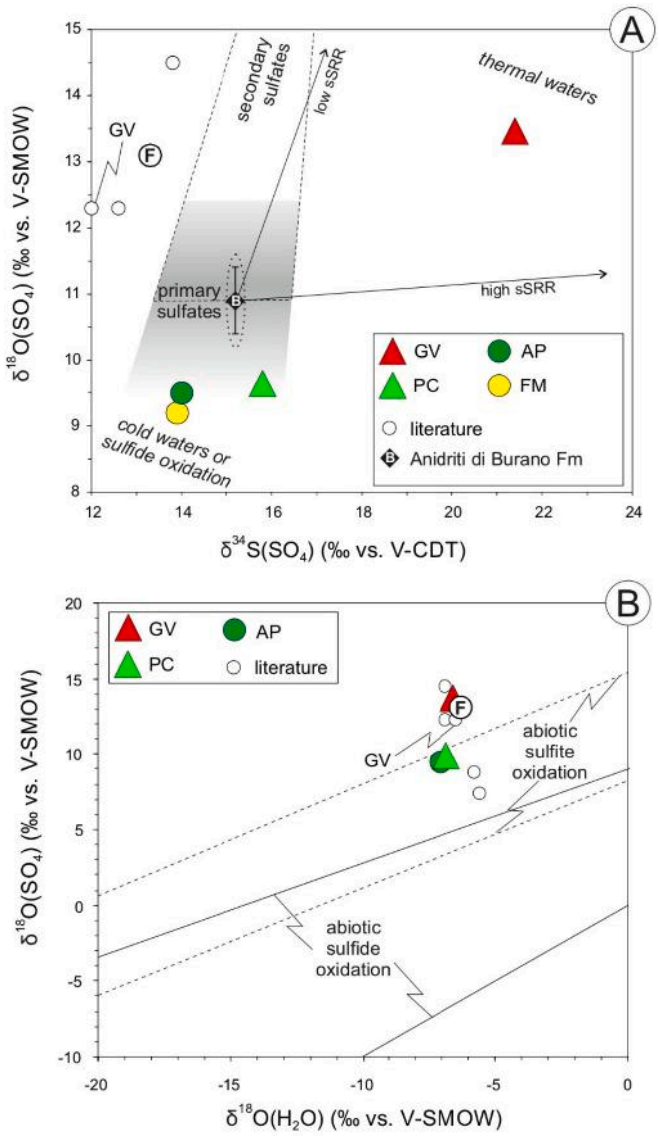

Fig. 10. (A) $\delta^{18}O(SO_4)$ versus $\delta^{34}S(SO_4)$ of the spring waters sampled in this study (colored circles) and the literature (small white circles; Governa et al., 1989; and F = Fogliano borehole). The gray area delimits the Upper Triassic "primary evaporite sulfate" values and the pooled standard deviation Upper Triassic sulfate minerals in the Apennine (gypsum and anhydrite of the *Anidriti di Burano* Formation), whereas the dotted ellipse delimits the C.I. at 99 % of the mean δ values (Boschetti et al., 2011). Low and high sSRR arrows depict the microbial cell-specific sulfate reduction rate (Brunner et al., 2005). (B) $\delta^{18}O(SO_4)$ versus $\delta^{34}S(SO_4)$ of the spring waters sampled in this study (colored circles) and the literature (small white circles; Governa et al., 1989). Broken and solid lines delimit areas of possible $\delta^{18}O$ paths for aqueous sulfate and water, the former obtained by inorganic oxidation of reduced sulfur involving or not involving sulfite as an intermediate form (Boschetti, 2013; van Stempvoort and Krouse, 1994). The abbreviations of the springs are listed in Table 1.

variability of the involved alumina silicates, which can affect the equilibrium activity of solids and thus the position of their stability limits, it is probable that the high K^+/H^+ activity ratios of the fluid samples from the Fogliano borehole (Fig. 7), as well as historical spring water samples, can be attributed to possible interactions with mica (muscovite) and K-feldspar (sanidine, which is not known in volcanic rocks of the area; c.f. Marra et al., 2021) (see Supplementary Material 1). Furthermore, all samples in this study exhibited undersaturation with respect to leucite. This mineral is not present in the diagrams, as it lies behind the sanidine field, and in any case, it is present only at temperatures exceeding 150 °C (at $T > 190$ °C with silica saturated by quartz). Therefore, it is undoubtedly risky to utilize a Na–K geothermometer where a generic K-feldspar is used as the sole K-bearing mineral phase. Moreover, the limits defined by Na^+/H^+ ratios are also difficult to attribute since the possible minerals involved may include (i) sodic zeolites, which are typically present in volcanic rocks such as (Na)-phillipsite or analcime, and (ii) albite (low) and quartz. The latter occur within the *Verrucano* and the *Anidriti di Burano* formations as well as in other crystalline basement units (e.g., Boschetti et al., 2017; Barberio et al., 2021). Another possible candidate could be pyroclastic *Peperino* units ($Na_2O < 3$ %; Civetta et al., 1981), which, together with lava dikes and flows, are distinctive of the tectonically controlled rooted centers of the Volsci Volcanic Field (Cardello et al., 2020; Marra et al., 2021; Fig. 2). These elements could extend to the edge of the Pontina Plain (Boni et al., 1980; Cardello et al., 2020). To help discriminate among these options, our estimates of the water origin could help predict their actual presence in the subsurface.

Concerning the Li, Rb, and Cs concentrations, the anomalies in GV, already noted in the PCA (Fig. 6), are also evident in the Li–Rb–Cs ternary diagram (Fig. 12). In particular, Fig. 12 illustrates how mixing with deep fluids that have interacted with the *Anidriti di Burano* Formation (Triassic evaporites) is not sufficient to explain the excess Cs, which could be related to magmatic rocks in the subsurface associated with the edging faults of the Pontina Plain (Fig. 7).

Thus, interactions with kamafugitic or phenolitic volcanic rocks are necessary. Elsewhere in the Apennines, it has been hypothesized that kamafugites such as those of the Cupaello eruptive center (c.f. Barberio et al., 2021) could result from interactions of meteoric or hydrothermal waters with carbonatites in equilibrium with alkaline silicate melts (Martin et al., 2012). Notably, one of the cesium-rich minerals found in volcanic rocks is pollucite, a feldspathoid isotypic with analcime and leucite, which is typically found in local volcanic rocks, whereas the former is commonly the alteration product of the latter.

Considering the activities of the dissolved species in the GV sample and a hypothetical equilibrium between analcime and pollucite:

$$\underset{\text{Pollucite}}{CsAlSi_2O_6} + 0.0303SiO_2(aq) + 1.01H_2O + Na^+ = \underset{\text{Analcime}}{1.01Na_{0.99}Al_{0.99}Si_{2.01}O_6 \bullet H_2O} + Cs^+$$

A temperature of approximately 40 °C is inferred (calculated via the Rxn tool of the GWB suite and the Thermoddem thermodynamic database). The same temperature can be obtained considering the mixing fractions of two endmembers, namely, Ca–HCO_3 water from the northern VR at $T = 11.0$ °C (Sappa and Tulipano, 2011) and Na–Cl water from the Fogliano borehole at 95.5 °C, 0.765 and 0.235, respectively, as calculated by the NetPath code for obtaining the GV water.

The calculation of gypsum saturation indices and the partial pressure of CO_2 in the water samples (both from this study and the literature) highlight how the values could be explained essentially by binary mixing between the waters from the northern VR and Na–Cl gypsum-saturated Fogliano deep fluids with $\log P(CO_2)g = 0.8$ (recalculated in this study at $T = 95.5$ °C and $P = 294$ bar; Supplementary Material 6). Similarly, the recalculation of the GV sample at $T = 40$ °C yielded the highest value for the sample spring, i.e., $\log P(CO_2)g = -0.8$, which confirms the contribution of CO_2 from a degassing mantle in the area (Minissale, 2004; Frondini et al., 2019). The exception is represented by shallow groundwater near the southern seashores of the Pontina Plain, which clearly mixes with seawater (Sappa et al., 2012). Furthermore, in some springs and sinkhole lakes, CO_2 anomalies that exceed mixing values may be caused by deep gas inputs (Panichi and Tongiorgi, 1976; Boni et al., 1980) (see Supplementary Material 7).

Therefore, as illustrated in Fig. 13, it could be hypothesized that GV waters, originating from mixing between deep Na–Cl-type fluids such as Fogliano and Ca–HCO_3 waters from the northern VR (i.e., Ninfa), may have reached equilibrium at the temperature resulting from interactions with leucite-bearing magmatic rocks (sensu Marra et al., 2021). This

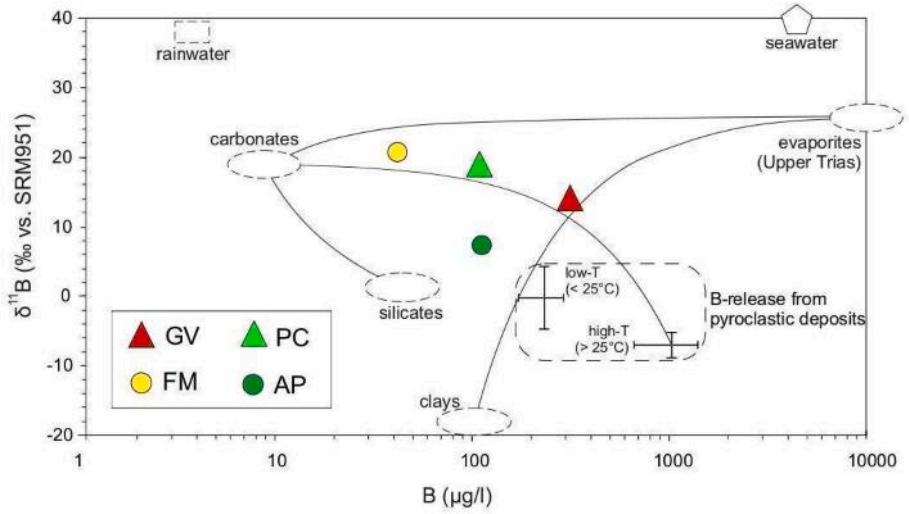

Fig. 11. $\delta^{11}B$ versus boron concentrations of four selected springs from the Pontina Plain. The dashed-contoured areas depict different and common boron sources (redrawn from Boschetti et al., 2019), and the solid curves represent the binary mixing between them. The abbreviations of the springs are listed in Table 1.

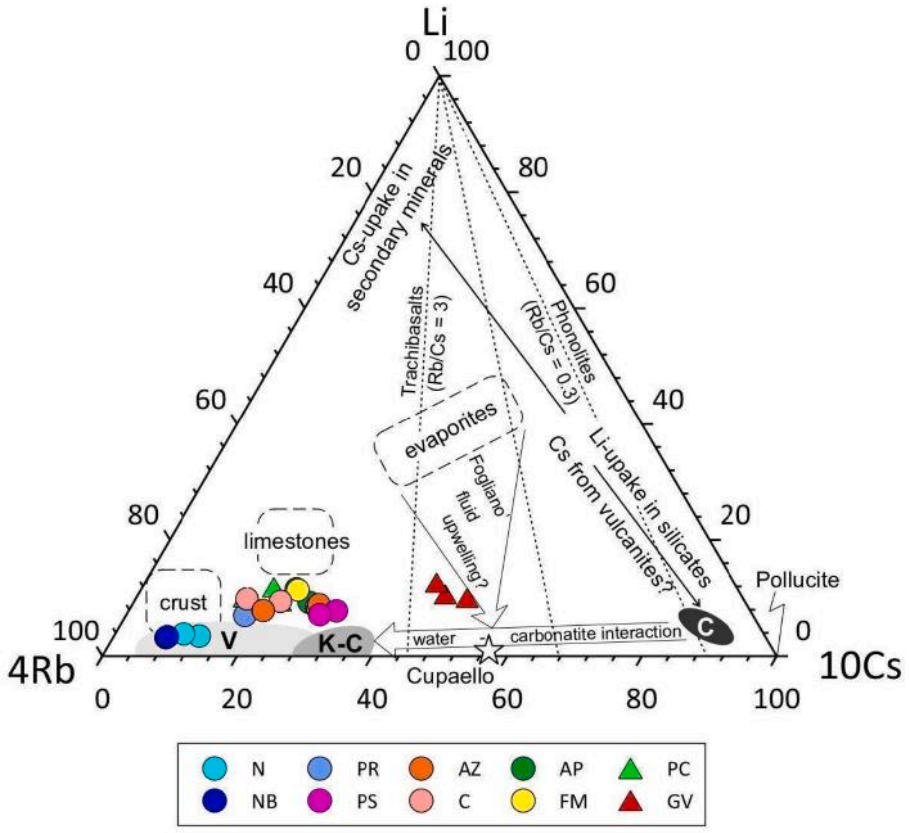

Fig. 12. Li–Rb–Cs ternary diagram of groundwater samples modified after Barberio et al. (2021). Dashed-contoured fields display the composition of average crust isochemical dissolution and water interacting with limestones and evaporites (Barberio et al., 2021). The V and K–C gray fields display the compositions of the vulcanites (Barnekov, 2000; Nikogosian and van Bergen, 2010) and kamafugites–carbonatites (Barberio et al., 2021) in the Roman magmatic province, respectively. The C-black field represents the theoretical carbonatites in equilibrium with alkaline silicate melts (Martin et al., 2012). The high-Cs Cupaello kamafugitic lavas (star; Stoppa and Cundari, 1995) and Rb/Cs ratios in trachibasalts and phonolites from Vico and Vulsini (Peccerillo, 2017) are also shown with dotted lines for comparison.

figure analyzes fault–controlled spring karst systems that, according to Keegan-Treloar et al. (2022), range from the local scale to the regional scale. The latter is the case for the fault structure edging the Pontina Plain, which, according to our evidence and seismostratigraphic analysis, is dominated by carbonates. Like the findings in the southern VR reported by Saroli et al. (2017) and Cuoco et al. (2017), in the northern VR, geothermal fluids may also create convective loops that trigger mixing between hot rising fluids and cold karstic water. Unlike the southern VR, where a strong magmatic component occurs within a complex fault–controlled mixing zone, in the northern VR, the magmatic component is less prevalent. Here, the hydrogeochemical signatures reveal that deep thermal water of meteoric origin interacted with

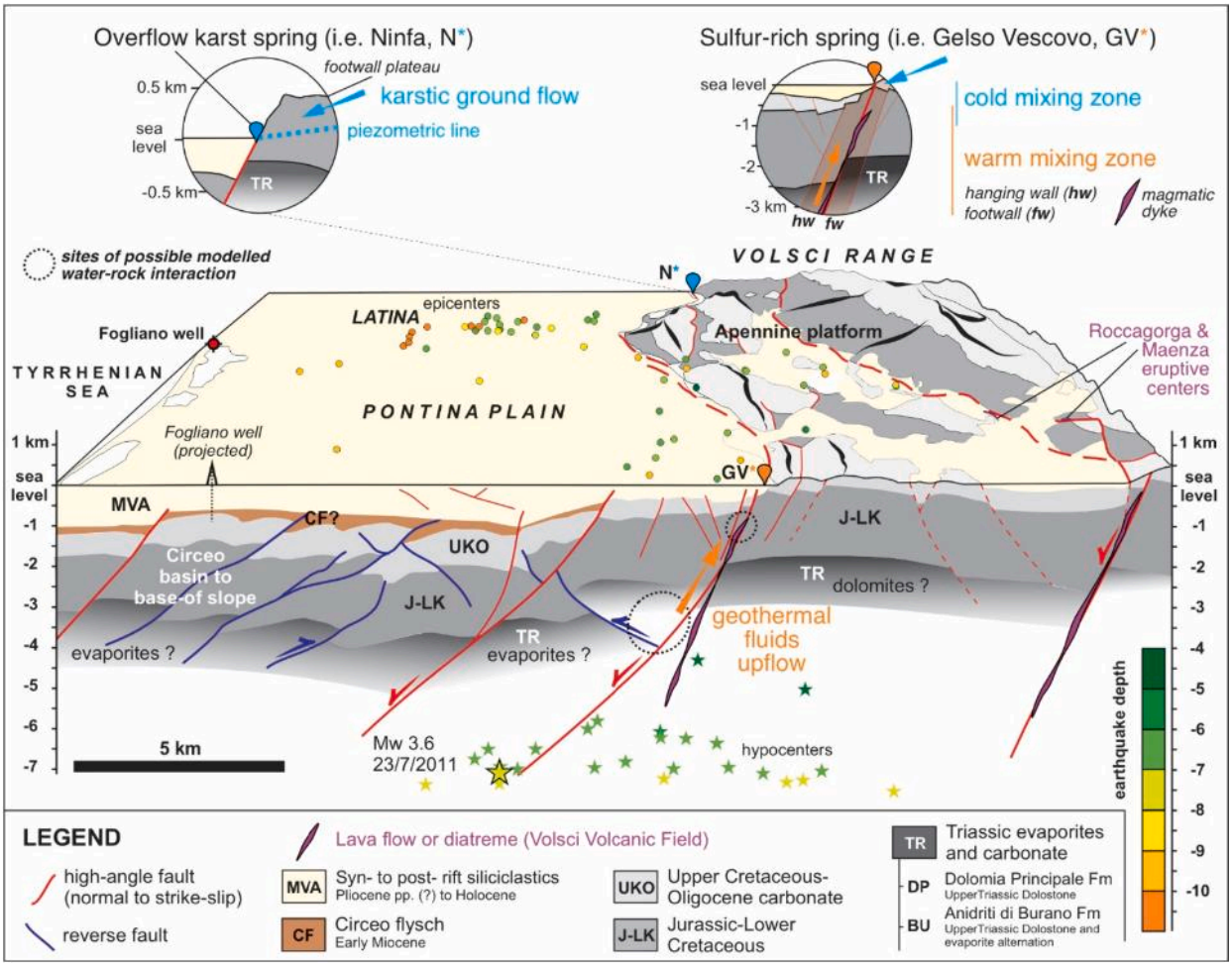

Fig. 13. Schematic 3D representation illustrating the mixing processes within the studied fault–controlled karstic aquifer, depicting interactions between deep thermal fluids and shallow groundwater from the northern Volsci Range (VR). The subsurface interpretation of the Pontina Plain is based on Fig. 7. As supported by the geochemical modeling results (Sections 5.2–5.4), the sketch highlights the potential influence of evaporites and magmatic rocks associated with the Volsci Volcanic Field (Cardello et al., 2020) on groundwater temperatures and compositions at various depths, which is supported by geochemical analyses and geothermometry. Earthquake locations are based on data from the INGV dataset (accessed on 1/05/2024, https://terremoti.ingv.it/) and highlight the shallower seismic activity at the edge between the VR and the Pontina Plain.

evaporitic and magmatic rocks. Furthermore, structural evidence of the fault structure (Figs. 3, 4) and neotectonic findings (Alessandri et al., 2021), which constrain basal groundwater flowpaths, act at the same time as preferential pathways for deep thermal fluid upflow, whose evidence is recorded at S-rich springs. As shown in Fig. 4, the travertine deposits surrounding the fault–controlled springs can provide a historical record of fault and spring discharge activity (e.g., Hancock et al., 1999; Brogi and Capezzuoli, 2009; Priestley et al., 2018) from a geological time perspective (see Brogi et al., 2012). Both morphostructural and stratigraphical observations, including speleothems, show that the present-day location of the springs (Figs. 2, 3, 4a) depends on prolonged interactions between climate and tectonics (see Section 2.2). However, the area also experiences ongoing karstic drainage evolution, represented by drained karst fields, sinkholes, and dolines occurring along high-angle fault zones. Furthermore, the young morphology, especially the N- and *E*-striking structures (Agostini, 1992; Faccenna, 1993), which commonly occur along the numerous springs distributed over a 25 km long front (c.f. Figs. 3f, 4f), confirms the immaturity of the drainage system, which, even in the driest seasons, results in sustained basal water flow, contrary to mature karst settings. The present-day fault activity, as three-dimensionally depicted in Fig. 13, is highlighted by the location of relatively low-magnitude earthquakes along the NW-striking faults bordering the Pontina Plain. Those are confined to depths of up to 6 km in the hanging wall, while reaching depths of approximately 4 km in the footwall. As this context is associated with degassing of deep-sourced CO_2 (Panichi and Tongiorgi, 1976; Boni et al., 1980) and considering their close relationship with seismic activity (Buttitta et al., 2023), further studies in this sense are encouraged.

The fault–controlled mixed groundwater karstic aquifer could serve as an example of similar structures in fold-and-thrust belts worldwide affected by alignments of karstic and variably diluted S-rich springs, such as those in the Jura mountains (e.g., Guglielmetti et al., 2022), where deeper interactions may also occur with the crystalline basement (c.f. Saroli et al., 2017). The VR–Pontina Plain example differs from the Jura mountains example because of the interactions with a K-bearing magmatic component, which has now been resolved with unprecedented detail and is worthy of further investigation.

Furthermore, identifying sites and processes related to groundwater mixing is crucial for effective management and environmental protection strategies of the resource over an area inhabited by 0.4 million people (https://www.regione.lazio.it/). This area is also home to significant agricultural and industrial activities that heavily benefit from and exploit water resources and are responsible for serious environmental and social impacts (Sappa et al., 2005), manifested by the substantial decline in piezometric levels and the increase in seawater intrusion (Manca et al., 2013). In addition to these local issues, ongoing

climate change may also impact groundwater quality (Sappa et al., 2014; Cioffi et al., 2017; Cappucci et al., 2024), which is influenced by a decrease in karstic aquifer recharge (Barbieri et al., 2021). Specifically, climate change effects can be enhanced in areas where the contribution of deep fluids is evident. Uprising fluids can enhance water–rock interactions (e.g., lowering the pH) and potentially promote the leaching and mobility of some dangerous trace elements (e.g., heavy metals, such as As; Chiarabba et al., 2022) (Supplementary Material 3) along the flowpath toward the surface. In particular, we point out that many springs display have As concentrations higher than the WHO guideline value of 10 ppb (WHO, 2022), reaching 32 ppb in the GV spring. Long-term hydrogeochemical monitoring is crucial and should be undertaken for detecting variations in groundwater quality, providing valuable information for stakeholders and the entire community.

6. Conclusions

To unravel the complex mixing interactions within one of the most representative fault–controlled mixed groundwater karstic aquifers in Central Italy, we integrated hydrogeochemical and isotopic analyses, framing them together with a structural review of the Pontina Plain. Field and seismic stratigraphic studies allowed us to extend our interpretations to depths of 5–7 km and provide insights into fault–fluid dynamics, contributing to mixing processes and multiple groundwater–rock interactions. This hydrogeological system has been evolving since at least the Late Pleistocene, as supported by our morphological and structural evidence.

Groundwater from the northern Volsci Range (VR) karst aquifer feeds springs with varying degrees of mineralization, exhibiting a discernible hydrogeological evolution from the Ca–HCO_3 hydrofacies to the Na–Cl hydrofacies, leading to the identification of three main spring groups on the basis primarily of their electrical conductivity (EC) values. The stable isotopes of water ($\delta^{18}O$-$\delta^{2}H$) in all the samples align with Latium meteoric water, indicating a meteoric origin predominantly recharged from the northern VR. The isotopic signatures of water molecules in the southernmost spring (GV), which is the most mineralized sampled spring, show enrichment in heavy isotopes, possibly linked to the inflow of deep meteoric waters that have been related to those measured at the Fogliano borehole. The latter, also of meteoric origin, is enriched because of recharge in the local coastal area. The calculated saturation indices, CO_2 partial pressures, and isotope ratios of strontium and sulfate consistently indicate that the hydrogeochemistry of the southernmost studied springs is a result of a mixing process with deep Na–Cl water, interacting with the *Anidriti di Burano* Triassic evaporites, and, during its ascent to the surface, mixed at a shallower portion of the crust with Ca–HCO_3 water from the karstic aquifer. This interpretation is supported by trace element concentrations (e.g., Li–Rb–Cs), with an excess of Cs possibly explained by interactions with ultrapotassic volcanic rocks such as pyroclastic deposits, lavas, or dikes. Through the application of chemical, isotope, and activity geothermometers, the equilibrium temperature of approximately 95.5 °C for the deep waters from the Fogliano borehole suggests a depth of deep fluids reservoir at 3 km, possibly in the evaporites (as supported by subsurface analysis), based on the geothermal gradient of the study area (30 °C/km). Additionally, a geochemical model simulation, which uses the calculated temperatures for the two endmembers (i.e., 95.5 °C for the deep Na–Cl fluids and 11 °C for the Ca–HCO_3 water from the northern VR), suggests that the mixing water may have reached equilibrium at 40 °C because of interactions with rooted magmatic rocks at an estimated depth of approximately 1 km within the otherwise carbonate-dominated fault structure edging the Pontina Plain.

Therefore, the complexity in the geochemical composition of the local springs is due not only to the varying degrees of mixing between shallow and deep components but also to the involvement of karst (carbonates), evaporites, and volcanic (silicates) products in the water–rock interaction processes, which occur at different temperatures and depths. Additionally, the calculation of mineral saturation indices and CO_2 partial pressures reveals that water–rock interactions are driven by an excess of deep (mantle) CO_2 dissolved in groundwater. The innovation of this study involves the use of trace elements and multiple isotope ratios (such as $^{87}Sr/^{86}Sr$, $\delta^{34}S(SO_4)$, $\delta^{18}O(SO_4)$, and $\delta^{11}B$) never before published for the area under investigation. In particular, strontium and sulfur isotopes elucidate the contributions of evaporites to water–rock interactions, whereas $\delta^{18}O(SO_4)$ and $\delta^{11}B$ values help trace the effects of temperature. Thus, this multi-isotopic approach significantly enriches the understanding of karstic hydrogeological systems. Moreover, our trace element results provide new insights into both the geological and environmental aspects of the study area: (i) cesium, a magmatic element, reveals a previously unexplored feature of the underlying geological environment, which aligns with the volcano–tectonic characteristics of the Volsci Volcanic Field; and (ii) As, a dangerous heavy metal, has concentrations that are higher than the WHO guideline value in many of the sampled springs, highlighting the importance of future long-term hydrogeochemical investigations to monitor potential changes in groundwater quality induced by climate change effects (i.e., a decrease in the contribution of rainfall to aquifer recharge with respect to deep-fluid contributions). Further research is warranted to explore deeper circulation patterns and refine hydrostructural model methodologies applied to similar settings worldwide.

Supplementary data to this article can be found online at https://doi.org/10.1016/j.scitotenv.2024.175439.

CRediT authorship contribution statement

Francesca Gori: Writing – original draft, Validation, Software, Methodology, Formal analysis, Data curation, Conceptualization. **Marino Domenico Barberio:** Writing – review & editing, Methodology, Investigation, Data curation. **Maurizio Barbieri:** Writing – review & editing, Validation, Supervision, Methodology. **Tiziano Boschetti:** Writing – review & editing, Writing – original draft, Validation, Supervision, Software, Methodology. **Giovanni Luca Cardello:** Writing – review & editing, Writing – original draft, Visualization, Validation, Software, Methodology, Investigation, Data curation, Conceptualization. **Marco Petitta:** Writing – review & editing, Validation, Supervision, Project administration, Methodology, Conceptualization.

Declaration of competing interest

The authors declare that they have no known competing financial interests or personal relationships that could have appeared to influence the work reported in this paper.

Data availability

All data are available in the manuscript and its related files

Acknowledgments

Institutional financial support from Sapienza University of Rome, Italy, is acknowledged: Sapienza Grant 2021, Intensive multiparametric monitoring of hydrogeological and hydrochemical data correlated with seismicity in Central-Southern Apennine (PI: Marco Petitta). Saverio D'Ottavi (Associazione Cavata Flumen), Angelo Giuliani, Riccardo Novaga, and Valeriano Aiello are thanked for their field support. We are also grateful to Giuseppe Vico and Mirko Carlini for their valuable insights on the subsurface interpretation of the area. We thank the editor Christian Herrera and two anonymous reviewers for having sensitively improved the manuscript impact. Open access funding provided by Università degli Studi di Sassari within the CRUI-CARE Agreement.

References

Accordi, B., 1966. La componente traslativa nella tettonica dell'Appennino laziale abruzzese. Geol. Romana 5, 355–406.

Accordi, G., Carbone, F., Civitelli, G., Corda, L., De Rita, D., Esu, D., Funiciello, R., Kotsakis, T., Mariotti, G., Sposato, A., 1988. Carta delle litofacies del Lazio-Abruzzo ed aree limitrofe. Note illustrative. CNR, Progetto Finalizzato Geodinamica, Quaderni de «La Ricerca Scientifica», Roma, 5, p. 114.

Agostini, S., 1992. Geologia e carsismo nei Monti Lepini – Atti XVI° congresso nazionale di Speleologia. Udine 1990. Le Grotte d'Italia, 16 (4), 59–68.

Alessandri, L., Cardello, G.L., Attema, P.A.J., Baiocchi, V., De Angelis, F., Del Pizzo, S., Di Ciaccio, F., Fiorillo, A., Gatta, M., Monti, F., Onori, M., Rolfo, M.F., Romboni, M., Sottili, G., Troisi, S., 2021. Reconstructing the Late Pleistocene–Anthropocene interaction between the neotectonic and archaeological landscape evolution in the Apennines (La Sassa cave, Italy). Quat. Sci. Rev. 265, 107067 https://doi.org/10.1016/j.quascirev.2021.107067.

Angelucci, A., 1966. La serie miocenica nella media Valle Latina (Frosinone). Geol. Romana 5, 425–452.

APAT IRSA-CNR, 2003. Metodi analitici per le acque 3030 Determinazione di cationi (Sodio, ammonio, potassio, magnesio, calcio) mediante cromatografia ionica, 1, 1153 pp.

Appelo, C.A.J., Postma, D., 2004. Geochemistry, Groundwater, and Pollution. CRC press. https://doi.org/10.1201/9781439833544.

Awaleh, M.O., Boschetti, T., Adaneh, A.E., Daoud, M.A., Ahmed, M.M., Dabar, O.A., Soubaneh, Y.D., Kawalieh, K.D., Kadieh, I.H., 2020. Hydrochemistry and multi-isotope study of the waters from Hanlé-Gaggadé grabens (Republic of Djibouti, East African Rift System): a low-enthalpy geothermal resource from a transboundary aquifer. Geothermics 86, 101805. https://doi.org/10.1016/j.geothermics.2020.101805.

Aydin, H., Karakuş, H., Mutlu, H., 2020. Hydrogeochemistry of geothermal waters in eastern Turkey: geochemical and isotopic constraints on water-rock interaction. J. Volcanol. Geotherm. Res. 390, 106708 https://doi.org/10.1016/j.jvolgeores.2019.106708.

Baird, R.B., Eaton, A.D., Rice, E.W., 2017. Standard Methods for Examination of Water and Wastewater, 23rd ed. American Public Health Association, American Water Works Association, Water Environment Federation, Washington D.C.

Bakalowicz, M., 2005. Karst groundwater: a challenge for new resources. Hydrogeol. J. 13, 148–160. https://doi.org/10.1007/s10040-004-0402-9.

Barberio, M.D., Gori, F., Barbieri, M., Boschetti, T., Caracausi, A., Cardello, G.L., Petitta, M., 2021. Understanding the origin and mixing of deep fluids in shallow aquifers and possible implications for crustal deformation studies: San Vittorino plain, central Apennines. Appl. Sci. 11 (4), 1353. https://doi.org/10.3390/app11041353.

Barbieri, M., Penta, A., Turi, B., 1975. Oxygen and strontium isotope ratios in some ejecta from the Alban Hills volcanic area, Roman comagmatic region. Contrib. Mineral. Petrol. 51, 127–133. https://doi.org/10.1007/BF00403753.

Barbieri, M., Boschetti, T., Petitta, M., Tallini, M., 2005. Stable isotope (2H, 18O and 87Sr/86Sr) and hydrochemistry monitoring for groundwater hydrodynamics analysis in a karst aquifer (Gran Sasso, Central Italy). Appl. Geochem. 20 (11), 2063–2081. https://doi.org/10.1016/j.apgeochem.2005.07.008.

Barbieri, M., Nigro, A., Petitta, M., 2017. Groundwater mixing in the discharge area of San Vittorino Plain (Central Italy): geochemical characterization and implication for drinking uses. Environ. Earth Sci. 76, 1–14. https://doi.org/10.1007/s12665-017-6719-1.

Barbieri, M., Franchini, S., Barberio, M.D., Billi, A., Boschetti, T., Giansante, L., Gori, F., Jónsson, S., Petitta, M., Skelton, A., Stockmann, G., 2021. Changes in groundwater trace element concentrations before seismic and volcanic activities in Iceland during 2010–2018. Sci. Total Environ. 793, 148635 https://doi.org/10.1016/j.scitotenv.2021.148635.

Barbieri, M., Barberio, M.D., Banzato, F., Billi, A., Boschetti, T., Franchini, S., Gori, F., Petitta, M., 2023. Climate change and its effect on groundwater quality. Environ. Geochem. Health 45 (4), 1133–1144. https://doi.org/10.1007/s10653-021-01140-5.

Barnekov, P., 2000. Volcanic Rocks from Central Italy: An Oxygen Isotopic Microanalytical and Geochemical Study. Ph.D. thesis. Georg-August-Universität, Göttingen.

Bense, V.F., Gleeson, T., Loveless, S.E., Bour, O., Scibek, J., 2013. Fault zone hydrogeology. Earth-Sci. Rev. 27, 171–192. https://doi.org/10.1016/j.earscirev.2013.09.008.

Bethke, C.M., Farrell, B., Yeakel, S., 2022. The Geochemist's Workbench® Release 12 - GWB Essentials Guide. Aqueous Solutions. LLC, Champaign, Illinois.

Blanc, P., Lassin, A., Piantone, P., Azaroual, M., Jacquemet, N., Fabbri, A., Gaucher, E.C., 2012. Thermoddem: a geochemical database focused on low temperature water/rock interactions and waste materials. Appl. Geochem. 27 (10), 2107–2116. https://doi.org/10.1016/j.apgeochem.2012.06.002.

Bojar, A.V., Chmiel, S., Bojar, H.P., Varlam, C., Barbu, V., 2021. Hydrological System in Quaternary Clastic Deposits, Mehedinti County, Romania: Isotope Composition, Chemistry and Radiocarbon Dating. https://doi.org/10.1144/SP507.

Boni, C., Bono, P., Calderoni, G., Lombardi, S., Turi, B., 1980. Indagine idrogeologica e geochimica sui rapporti tra ciclo carsico e circuito idrotermale nella pianura pontina (Lazio meridionale). Geol. Appl. Idrogeol. 15, 203–247. Bari.

Bono, P., 1981. Valutazione preliminare del potenziale geotermico della regione laziale. Geol. Romana 20, 69–78.

Bono, P., 1995. The sinkhole of Doganella (Pontina Plain, Central Italy). Environ. Geol. 26, 48–52. https://doi.org/10.1007/BF00776031.

Bono, P., 2011. Valutazione delle risorse idriche naturalmente rinnovabili, caratterizzazione chimica ed isotopica delle acque sorgentizie e sotterranee, condizioni ai limiti. In: Provincia di Latina, Progetto Monti Lepini: Studi idrogeologici per la tutela e la gestione della risorsa idrica. Gangemi Editore, Roma, p. 143.

Boschetti, T., 2013. Oxygen isotope equilibrium in sulfate–water systems: a revision of geothermometric applications in low-enthalpy systems. J. Geochem. Explor. 124, 92–100. https://doi.org/10.1016/j.gexplo.2012.08.011.

Boschetti, T., Iacumin, P., 2005. Continuous-flow δ18O measurements: new approach to standardization, high-temperature thermodynamic and sulfate analysis. Rapid Commun. 19 (21), 3007–3014. https://doi.org/10.1002/rcm.2161.

Boschetti, T., Cortecci, G., Bolognesi, L., 2003. Chemical and isotopic compositions of the shallow groundwater system of Vulcano Island, Aeolian Archipelago, Italy: an update. GeoActa 2, 1–34.

Boschetti, T., Venturelli, G., Toscani, L., Barbieri, M., Mucchino, C., 2005. The Bagni di Lucca thermal waters (Tuscany, Italy): an example of Ca-SO4 waters with high Na/Cl and low Ca/SO4 ratios. J. Hydrol. 307 (1–4), 270–293. https://doi.org/10.1016/j.jhydrol.2004.10.015.

Boschetti, T., Cortecci, G., Toscani, L., Iacumin, P., 2011. Sulfur and oxygen isotope compositions of Upper Triassic sulfates from Northern Apennines (Italy): palaeogeographic and hydrogeochemical implications. Geol. Acta 129–147. https://doi.org/10.1344/105.000001690.

Boschetti, T., Toscani, L., Barbieri, M., Mucchino, C., Marino, T., 2017. Low enthalpy Na-chloride waters from the Lunigiana and Garfagnana grabens, Northern Apennines, Italy: tracing fluid connections and basement interactions via chemical and isotopic compositions. J. Volcanol. Geotherm. Res. 348, 12–25. https://doi.org/10.1016/j.jvolgeores.2017.10.008.

Boschetti, T., Barbieri, M., Barberio, M.D., Billi, A., Franchini, S., Petitta, M., 2019. CO_2 inflow and elements desorption prior to a seismic sequence, Amatrice-Norcia 2016, Italy. Geochem. Geophys. Geosyst. 20 (5), 2303–2317. https://doi.org/10.1029/2018GC008117.

Boschetti, T., Barbieri, M., Barberio, M.D., Skelton, A., Stockmann, G., Toscani, L., 2022. Geothermometry and water–rock interaction modelling at Hafralækur: possible implications of temperature and CO_2 on hydrogeochemical changes previously linked to earthquakes in northern Iceland. Geothermics 105, 102535. https://doi.org/10.1016/j.geothermics.2022.102535.

Boschetti, T., Salvioli-Mariani, E., Toscani, L., 2024. Lithium-rich basement brines: activity versus concentration geothermometry. Geothermics 119, 102965. https://doi.org/10.1016/j.geothermics.2024.102965.

Branson, O., 2018. Boron incorporation into marine $CaCO_3$. In: Marschall, H., Foster, G. (Eds.), Boron Isotopes: The Fifth Element, Advances in Isotope Geochemistry. Springer International Publishing, pp. 71–105. https://doi.org/10.1007/978-3-319-64666-4_4.

Brogi, A., Capezzuoli, E., 2009. Travertine deposition and faulting: the fault-related travertine fissure-ridge at Terme S. Giovanni, Rapolano Terme (Italy). Int. J. Earth Sci. 98, 931–947. https://doi.org/10.1007/s00531-007-0290-z.

Brogi, A., Capezzuoli, E., Buracchi, E., Branca, M., 2012. Tectonic control on travertine and calcareous tufa deposition in a low-temperature geothermal system (Sarteano, Central Italy). J. Geol. Soc. Lond. 169 (4), 461–476. https://doi.org/10.1144/0016-76492011-137.

Brunner, B., Bernasconi, S.M., Kleikemper, J., Schroth, M.H., 2005. A model for oxygen and sulfur isotope fractionation in sulfate during bacterial sulfate reduction processes. Geochim. Cosmochim. Acta 69 (20), 4773–4785. https://doi.org/10.1016/j.gca.2005.04.017.

Buttitta, D., Capasso, G., Paternoster, M., Barberio, M.D., Gori, F., Petitta, M., Picozzi, M., Caracausi, A., 2023. Regulation of deep carbon degassing by gas-rock-water interactions in a seismic region of Southern Italy. Sci. Total Environ. 897, 165367 https://doi.org/10.1016/j.scitotenv.2023.165367.

Camponeschi, B., Nolasco, F., 1983. Le risorse naturali della Regione Lazio – Monti Lepini e Pianura Pontina. Regione Lazio, 8.

Capelli, G., Mastrorillo, L., Mazza, R., Petitta, M., Baldoni, T., Banzato, F., Cascone, D., Di Salvo, C., La Vigna, F., Taviani, S., Teoli, P., 2012. Carta Idrogeologica del Territorio della Regione Lazio, scala 1:100000 (4 fogli). Regione Lazio. S.EL.CA., Firenze.

Cappucci, S., Carillo, A., Iacono, R., Moretti, L., Palma, M., Righini, G., Antonioli, F., Sannino, G., 2024. Evolution of coastal environments under inundation scenarios using an oceanographic model and remote sensing data. Remote Sens. (Basel) 16, 2599. https://doi.org/10.3390/rs16142599.

Carapezza, M.L., Barberi, F., Ranaldi, M., Ricci, T., Tarchini, L., Barrancos, J., Fischer, C., Granieri, D., Lucchetti, C., Melian, G., Perez, N., Tuccimei, P., Vogel, A., Weber, K., 2012. Hazardous gas emissions from the flanks of the quiescent Colli Albani volcano (Rome, Italy). Appl. Geochem. 27 (9), 1767–1782. https://doi.org/10.1016/j.apgeochem.2012.02.012.

Cardello, G.L., Doglioni, C., 2015. From mesozoic rifting to Apennine orogeny: the gran Sasso range (Italy). Gondwana Res. 27 (4), 1307–1334. https://doi.org/10.1016/j.gr.2014.09.009.

Cardello, G.L., Consorti, L., Palladino, D.M., Carminati, E., Carlini, M., Doglioni, C., 2020. Tectonically controlled carbonate-seated maar-diatreme volcanoes: the case of the Volsci Volcanic Field, central Italy. J. Geodyn. 139, 101763 https://doi.org/10.1016/j.jog.2020.101763.

Cardello, G.L., Vico, G., Consorti, L., Sabbatino, M., Carminati, E., Doglioni, C., 2021. Constraining the passive to active margin tectonics of the internal central Apennines: insights from biostratigraphy, structural, and seismic analysis. Geosciences 11 (4), 160. https://doi.org/10.3390/geosciences11040160.

Cardello, G.L., Tomassetti, L., Cornacchia, I., Mancini, A., Mancini, M., Mazzini, I., Rusciadelli, G., Capezzuoli, E., Lorenzi, V., Petitta, M., Cavinato, G.P., Girotti, O., Brandano, M., 2022. The Tethyan and Tyrrhenian margin record of the Central

Apennines: a guide with insights from stratigraphy, tectonics, and hydrogeology. Geol. Field Trips Maps 14 (2.2), 1–113. https://doi.org/10.3301/gft.2022.05.
Cardello, G.L., Bernasconi, S.M., Fellin, M.G., Rahn, M., Rosskopf, R., Maden, C., Mancktelow, N.S., 2024. Carbonate deformation through the brittle-ductile transition: the case of the SW Helvetic nappes, Switzerland. J. Struct. Geol. 181, 105083 https://doi.org/10.1016/j.jsg.2024.105083, 24 pages.
Carminati, E., Doglioni, C., 2012. Alps vs. Apennines: the paradigm of a tectonically asymmetric Earth. Earth Sci. Rev. 112 (1–2), 67–96. https://doi.org/10.1016/j.earscirev.2012.02.004.
Celico, P., 1980. Le sorgenti della Piana di Fondi (Lazio Meridionale): prime considerazioni idrogeologiche in base al chimismo delle acque. Boll. Soc. dei Naturalisti in Napoli 89, 255–267.
Celico, P., Gonfiantini, R., Koizumi, M., Mangano, F., 1984. Environmental isotope studies of limestone aquifers in central Italy. In: International Symposium on Isotope Hydrology in Water Resources Development, 6, pp. 173–192. Vienna (Austria); 12-16 Sep 1983; IAEA-SM–270/24.
Centamore, E., Di Manna, P., Rossi, D., 2007. Kinematic evolution of the Volsci range: a new overview. Ital. J. Geosci. 126, 159–172.
Chiarabba, C., De Gori, P., Valoroso, L., Petitta, M., Carminati, E., 2022. Large extensional earthquakes push-up terrific amount of fluids. Sci. Rep. 12 (1), 14597 https://doi.org/10.1038/s41598-022-18688-6.
Chiodini, G., Cardellini, C., Amato, A., Boschi, E., Caliro, S., Frondini, F., Ventura, G., 2004. Carbon dioxide Earth degassing and seismogenesis in central and southern Italy. Geophys. Res. Lett. 31 (7) https://doi.org/10.1029/2004GL019480.
Cioffi, F., Conticello, F., Lall, U., Marotta, L., Telesca, V., 2017. Large scale climate and rainfall seasonality in a Mediterranean area: insights from a non-homogeneous Markov model applied to the Agro-Pontino plain. Hydrol. Process. 31 (3), 668–686. https://doi.org/10.1002/hyp.11061.
Cioni, R., Marini, L., 2020. A Thermodynamic Approach to Water Geothermometry. Springer, Berlin/Heidelberg, Germany, p. 415.
Civetta, L., Innocenti, F., Manetti, P., Peccerillo, A., Poli, G., 1981. Geochemical characteristics of potassic volcanics from Mts. Ernici (southern Latium, Italy). Contrib. Mineral. Petrol. 78, 37–47. https://doi.org/10.1007/BF00371142.
Civita, M., 1972. Schematizzazione idrogeologica delle sorgenti normali e delle relative opere di captazione. In: Memorie e Note dell'istituto di geologia applicata n. 12, Napoli.
Cloetingh, S.A.P.L., Burov, E., Matenco, L., Toussaint, G., Bertotti, G., Andriessen, P.A.M., Wortel, M.J.R., Spakman, W., 2004. Thermo-mechanical controls on the mode of continental collision in the SE Carpathians (Romania). Earth Planet. Sci. 218 (1–2), 57–76. https://doi.org/10.1016/S0012-821X(03)00645-9.
Cosentino, D., Cipollari, P., Di Donato, V., Sgrosso, I.S.M., 2002. The Volsci range in the kinematic evolution of the northern and southern Apennine orogenic system. Boll. Soc. Geol. Ital. 1 (1), 209–218. Special volume.
Cuoco, E., Minissale, A., Di Leo, A.M., Tamburrino, S., Iorio, M., Tedesco, D., 2017. Fluid geochemistry of the Mondragone hydrothermal systems (southern Italy): water and gas compositions vs. geostructural setting. Int. J. Earth Sci. 106, 2429–2444. https://doi.org/10.1007/s00531-016-1439-4.
Deffenu, L., Lombardi, S., Federici, C., 1975. An introductory note on statistical analysis of physio-chemical characteristics of natural waters. In: Application to Some Central Apennines Spring Waters. Atti della Accademia Nazionale dei Lincei. Classe di Scienze Fisiche, Matematiche e Naturali. Rendiconti, 59, pp. 125–139. http://gdmltest.u-ga.fr/item/RLINA_1975_8_59_1-2_125_0/.
Delchiaro, M., Fioramonti, V., Della Seta, M., Cavinato, G.P., Mattei, M., 2021. Fluvial inverse modeling for inferring the timing of Quaternary uplift in the Simbruini range (Central Apennines, Italy). Trans. GIS 25 (5), 2455–2480. https://doi.org/10.1111/tgis.12833.
Deng, J., Yang, G., Yan, X., Du, J., Tang, Q., Yu, C., Pu, S., 2024. Quality evaluation and health risk assessment of karst groundwater in Southwest China. Sci. Total Environ. 946 https://doi.org/10.1016/j.scitotenv.2024.174371, 174371. page 13.
Doummar, J., Sauter, M., Geyer, T., 2012. Simulation of flow processes in a large scale karst system with an integrated catchment model (Mike She)–identification of relevant parameters influencing spring discharge. J. Hydrol. 426, 112–123. https://doi.org/10.1016/j.jhydrol.2012.01.021.
Duchi, V., Paolieri, M., Pizzetti, A., 1991. Geochemical study on natural gas and water discharges in the Southern Latium (Italy): circulation, evolution of fluids and geothermal potential in the region. J. Volcanol. Geotherm. Res. 47 (3–4), 221–235. https://doi.org/10.1016/0377-0273(91)90002-H.
Faccenna, C., 1993. Tettonica quaternaria e stili deformativi lungo il margine tirrenico laziale. – PhD Thesis. Department of Earth Sciences, "La Sapienza" Roma.
Faulds, J.E., Coolbaugh, M.F., Vice, G.S., Edwards, M.L., 2006. Characterizing structural controls of geothermal fields in the northwestern Great Basin: a progress report. Trans. - Geotherm. Resour. Counc. 30, 69–76.
Federici, P.R., 1979. Una ipotesi di cronologia glaciale wurmiana, tardo e post-wurmiana nell'Appennino centrale. Geogr. Fis. Din. Quat. 2 (1979), 196–202.
Fellin, M.G., San Jose, M., Faccenna, C., Willett, S.D., Cosentino, D., Lanari, R., Goubert, L., Maden, C., 2022. Transition from slab roll-back to slab break-off in the central Apennines, Italy: constraints from the stratigraphic and thermochronologic record. GSA Bull. 134 (7–8), 1916–1930. https://doi.org/10.1130/B36123.1.
Fiori, C., 2007. Geochemical and Isotopic Approach for Precipitation and Groundwater in Central Italy. Università degli Studi di Roma, La Sapienza. Ph.D. Thesis.
Ford, D., Williams, P.D., 2007. Karst Hydrogeology and Geomorphology. John Wiley & Sons.
Frondini, F., Cardellini, C., Caliro, S., Beddini, G., Rosiello, A., Chiodini, G., 2019. Measuring and interpreting CO_2 fluxes at regional scale: the case of the Apennines, Italy. J. Geol. Soc. 176 (2), 408–416. https://doi.org/10.1144/jgs2017-169.
Gat, J.R., Carmi, I., 1970. Evolution of the isotopic composition of atmospheric waters in the Mediterranean Sea area. J. Geophys. Res. 75 (15), 3039–3048. https://doi.org/10.1029/JC075i015p03039.
Giggenbach, W.F., Minissale, A.A., Scandiffio, G., 1988. Isotopic and chemical assessment of geothermal potential of the Colli Albani area, Latium region, Italy. Appl. Geochem. 3 (5), 475–486. https://doi.org/10.1016/0883-2927(88)90020-0.
Goldscheider, N., Madl-Szny, J., Erss, A., Schill, E., 2010. Thermal water resources in carbonate rock aquifers. Hydrogeol. J. 18 (6), 1303. https://doi.org/10.1007/s10040-010-0611-3.
Gori, F., Paternoster, M., Barbieri, M., Buttitta, D., Caracausi, A., Parente, F., Sulli, A., Petitta, M., 2023. Hydrogeochemical multi-component approach to assess fluids upwelling and mixing in shallow carbonate-evaporitic aquifers (Contursi area, southern Apennines, Italy). J. Hydrol. 618, 129258 https://doi.org/10.1016/j.jhydrol.2023.129258.
Gourcy, L.L., Groening, M., Aggarwal, P.K., 2005. Stable oxygen and hydrogen isotopes in precipitation. In: Aggarwal, P.K., Gat, J.R., Froehlich, K.F.O. (Eds.), Isotopes in the Water Cycle: Past, Present and Future of Developing Science. Springer, Dordrecht, the Netherlands, pp. 39–51. https://doi.org/10.1007/1-4020-3023-1_4.
Governa, M.E., Masciocco, L., Riba, M., Zuppi, G.M., Lombardi, S., 1989. 1989. Karst and geothermal water circulation in the Central Apennines (Italy). In: Isotope Techniques in the Study of the Hydrology of Fractured and Fissured Rocks. International Atomic Energy Agency, Vienna, Austria.
Guglielmetti, L., Heidinger, M., Eichinger, F., Moscariello, A., 2022. Hydrochemical characterization of groundwaters' fluid flow through the upper mesozoic carbonate geothermal reservoirs in the Geneva Basin: an evolution more than 15,000 years long. Energies 15 (10), 3497. https://doi.org/10.3390/en15103497.
Hancock, P.L., Chalmers, R.M.L., Altunel, E., Çakir Travitonics, Z., 1999. Using travertines in active fault studies. J. Struct. Geol. 21, 903–916. https://doi.org/10.1016/S0191-8141(99)00061-9.
Holland, T.J.B., Powell, R., 2011. An improved and extended internally consistent thermodynamic dataset for phases of petrological interest, involving a new equation of state for solids. J. Metamorph. Geol. 29 (3), 333–383. https://doi.org/10.1111/j.1525-1314.2010.00923.x.
Holmslykke, H.D., Schovsbo, N.H., Kristensen, L., Weibel, R., Nielsen, L.H., 2019. Characterising brines in deep Mesozoic sandstone reservoirs. Denmark. GEUS Bull. 43 https://doi.org/10.34194/GEUSB-201943-01-04.
Horita, J., Kendall, C., 2004. Stable isotope analysis of water and aqueous solutions by conventional dual-inlet mass spectrometry. In: De Groot, P.A. (Ed.), Handbook of Stable Isotope Analytical Techniques, 1. Elsevier Amsterdam, The Netherlands, pp. 1–37. https://doi.org/10.1016/B978-044451114-0/50003-X. Chapter 1.
Jolie, E., Klinkmueller, M., Moeck, I., 2015. Diffuse surface emanations as indicator of structural permeability in fault–controlled geothermal systems. J. Volcanol. Geotherm. Res. 290, 97–113. https://doi.org/10.1016/j.jvolgeores.2014.11.003.
Keegan-Treloar, R., Irvine, D.J., Solórzano-Rivas, S.C., Werner, A.D., Banks, E.W., Currell, M.J., 2022. fault–controlled springs: a review. Earth-Sci. Rev. 230, 104058 https://doi.org/10.1016/j.earscirev.2022.104058, pp. 18.
Köppen, W., Geiger, R., 1930. Handbuch der klimatologie, 1. Gebrüder Borntraeger, Berlin.
Lacroix, B., Baumgartner, L.P., Bouvier, A.S., Kempton, P.D., Vennemann, T., 2018. Multi fluid-flow record during episodic mode I opening: a microstructural and SIMS study (Cotiella Thrust Fault, Pyrenees). Earth Planet. Sci. Lett. 503, 37–46. https://doi.org/10.1016/j.epsl.2018.09.016.
Li, X., Huang, X., Liao, X., Zhang, Y., 2020. Hydrogeochemical characteristics and conceptual model of the geothermal waters in the Xianshuihe fault zone, southwestern China. Int. J. Environ. Res. Public Health 17 (2), 500. https://doi.org/10.3390/ijerph17020500.
Liu, Y., Yamanaka, T., 2012. Tracing groundwater recharge sources in a mountain–plain transitional area using stable isotopes and hydrochemistry. J. Hydrol. 464, 116–126. https://doi.org/10.1016/j.jhydrol.2012.06.053.
Longinelli, A., Selmo, E., 2003. Isotopic composition of precipitation in Italy: a first overall map. J. Hydrol. 270 (1–2), 75–88. https://doi.org/10.1016/S0022-1694(02)00281-0.
Lorenzi, V., Banzato, F., Barberio, M.D., Goeppert, N., Goldscheider, N., Gori, F., Lacchini, A., Manetta, M., Medici, G., Rusi, S., Petitta, M., 2024. Tracking flowpaths in a complex karst system through tracer test and hydrogeochemical monitoring: implications for groundwater protection (Gran Sasso, Italy). Heliyon 10 (2). https://doi.org/10.1016/j.heliyon.2024.e24663.
Manca, F., Gragnanini, V., Capelli, G., Mazza, R., 2013. Seawater intrusion in a coastal area: one year experimental results between Fogliano and Caprolace Lakes (Pontina Plain - Latina). Rend. Online Soc. Geol. It. 24, 199–201.
Marra, F., Cardello, G.L., Gaeta, M., Jicha, B.R., Montone, P., Niespolo, E.M., Nomade, S., Palladino, D.M., Pereira, A., De Luca, G., Florindo, F., Frepoli, A., Renne, P.R., Sottili, G., 2021. The Volsci Volcanic Field (central Italy): eruptive history, magma system and implications on continental subduction processes. Int. J. Earth Sci. 110, 689–718. https://doi.org/10.1007/s00531-021-01981-6.
Martin, L.H., Schmidt, M.W., Mattsson, H.B., Ulmer, P., Hametner, K., Günther, D., 2012. Element partitioning between immiscible carbonatite–kamafugite melts with application to the Italian ultrapotassic suite. Chem. Geol. 320, 96–112. https://doi.org/10.1016/j.chemgeo.2012.05.019.
McArthur, J.M., Howarth, R.J., Shields, G.A., Zhou, Y., 2020. Sr-isotope stratigraphy, chapter 7. In: Gradstein, F.M., Ogg, J.G., Schmitz, M.D., Ogg, G.M. (Eds.), Geologic Time Scale 2020, 1. Elsevier, pp. 211–238.
Medici, G., Lorenzi, V., Sbarbati, C., Manetta, M., Petitta, M., 2023. Structural classification, discharge statistics, and recession analysis from the springs of the Gran Sasso (Italy) carbonate aquifer; comparison with selected analogues worldwide. Sustainability 15 (13), 10125. https://doi.org/10.3390/su151310125.

Milia, A., Torrente, M.M., 2015. Tectono-stratigraphic signature of a rapid multistage subsiding rift basin in the Tyrrhenian-Apennine hinge zone (Italy): a possible interaction of upper plate with subducting slab. J. Geodyn. 86, 42–60. https://doi.org/10.1016/j.jog.2015.02.005.

Milia, A., Torrente, M.M., Tesauro, M., 2017. From stretching to mantle exhumation in a triangular backarc basin (Vavilov basin, Tyrrhenian Sea, western Mediterranean). Tectonophysics 710, 108–126. https://doi.org/10.1016/j.tecto.2016.10.017.

Minissale, A., 2004. Origin, transport and discharge of CO_2 in central Italy. Earth Sci. Rev. 66 (1–2), 89–141. https://doi.org/10.1016/j.earscirev.2003.09.001.

Moreno-Gómez, M., Liedl, R., Stefan, C., Pacheco, J., 2023. Theoretical analysis and considerations of the main parameters used to evaluate intrinsic karst groundwater vulnerability to surface pollution. Sci. Total Environ. 907, 167947 https://doi.org/10.1016/j.scitotenv.2023.167947 pages 15.

Mostardini, F., Merlini, S., 1988. Appennino Centro Meridionale. In: Atti del 73 Congresso della Società Geologica Italiana: Geologica dell'Italia centrale: Roma, 30 Settembre-4 Ottobre 1986, 135 (2). Memorie della Società Geologica Italiana, pp. 187–202.

Nicholson, K., 1993. Geothermal Fluids: Chemistry and Exploration Techniques. Springer Science & Business Media. https://doi.org/10.1007/978-3-642-77844-5.

Nikogosian, I.K., van Bergen, M.J., 2010. Heterogeneous mantle sources of potassium-rich magmas in central-southern Italy: melt inclusion evidence from Roccamonfina and Ernici (Mid Latina Valley). J. Volcanol. Geotherm. Res. 197 (1–4), 279–302. https://doi.org/10.1016/j.jvolgeores.2010.06.014.

Nisio, S., 2008. I sinkholes nel Lazio - the sinkholes in the Latium region. Mem. Descr. Carta Geol. d'It. 85, 33–148.

Ogorodova, L.P., Melchakova, L.V., Kiseleva, I.A., Belitsky, I.A., 2003. Thermochemical study of natural pollucite. Thermochim. Acta 403 (2), 251–256. https://doi.org/10.1016/S0040-6031(03)00048-0.

Ortner, H., Reiter, F., Acs, P., 2002. Easy handling of tectonic data: the programs TectonicVB for Mac and TectonicsFP for Windows™. Comput. Geosci. 28 (10), 1193–1200. https://doi.org/10.1016/S0098-3004(02)00038-9.

Panichi, C., Tongiorgi, E., 1976. Carbon isotopic composition of CO2 from springs, fumaroles, mofettes and travertines of central and southern Italy: a preliminary prospection method of geothermal area. In: Proc. 2nd UN Symp. on the Develop and Use of Geotherm. Energy, 20–29 May 1975, San Francisco, U.S.A, pp. 815–825.

Parkhurst, D.L., Appelo, C.A.J., 2013. Description of input and examples for PHREEQC Version 3 - a computer program for speciation, batch-reaction, one-dimensional transport, and inverse geochemical calculations. In: U.S. Geological Survey Techniques and Methods book 6, chap. A43 497 p., available only at. http://pubs.usgs.gov/tm/06/a43/.

Parkhurst, D.L., Charlton, S.R., 2008. NetpathXL – an excel Interface to the program NETPATH. In: U.S. Geological Survey Techniques and Methods 6-A26, Reston, Virginia, 11 p. available only at. https://pubs.usgs.gov/tm/06A26/.

Peccerillo, A., 2017. Cenozoic Volcanism in the Tyrrhenian Sea Region, 2nd Edition. In: Advances in Volcanology Series. Springer International Publishing AG. 399 pp.

Petitta, 1994. Modelli matematici di simulazione dell'acquifero carsico dei Monti Lepini (Lazio meridionale). PhD Thesis. Sapienza University. February 1994.

Petitta, M., Primavera, P., Tuccimei, P., Aravena, R., 2011. Interaction between deep and shallow groundwater systems in areas affected by Quaternary tectonics (Central Italy): a geochemical and isotope approach. Environ. Earth Sci. 63, 11–30. https://doi.org/10.1007/s12665-010-0663-7.

Piscopo, V., Barbieri, M., Monetti, V., Pagano, G., Pistoni, S., Ruggi, E., Stanzione, D., 2006. Hydrogeology of thermal waters in Viterbo area, central Italy. Hydrogeol. J. 14, 1508–1521. https://doi.org/10.1007/s10040-006-0090-8.

Pizzino, L., 2015. Fluid Geochemistry and Natural Gas Hazard in the Urban Area of Rome. Università degli studi Roma Tre. Ph.D. Thesis.

Priestley, S.C., Karlstrom, K.E., Love, A.J., Crossey, L.J., Polyak, V.J., Asmerom, Y., Meredith, K.T., Crow, R., Keppel, M.N., Habermehl, M.A., 2018. Uranium series dating of Great Artesian Basin travertine deposits: implications for palaeohydrogeology and palaeoclimate. Palaeogeogr. Palaeoclimatol. Palaeoecol. 490, 163–177. https://doi.org/10.1016/j.palaeo.2017.10.024.

Rovida, A., Locati, M., Camassi, R., Lolli, B., Gasperini, P., 2020. The Italian earthquake catalogue CPTI15. Bull. Earthq. Eng. 18, 2953–2984. https://doi.org/10.1007/s10518-020-00818-y.

Salvati, R., Sasowsky, I.D., 2002. Development of collapse sinkholes in areas of groundwater discharge. J. Hydrol. 264 (1–4), 1–11. https://doi.org/10.1016/S0022-1694(02)00062-8.

Sanjuan, B., Millot, R., Asmundsson, R., Brach, M., Giroud, N., 2014. Use of two new Na/Li geothermometric relationships for geothermal fluids in volcanic environments. Chem. Geol. 389, 60–81. https://doi.org/10.1016/j.chemgeo.2014.09.011.

Sappa, G., Coviello, M.T., 2012. Seawater intrusion and salinization processes assessment in a multistrata coastal aquifer in Italy. J. Water Resour. Prot. 4 (11) https://doi.org/10.4236/jwarp.2012.411111.

Sappa, G., Tulipano, L., 2011. In: Lambrakis, N., Stournaras, G., Katsanou, K. (Eds.), Advances in the Research of Aquatic Environment, 1. Springer, Berlin Heidelberg, pp. 399–406. https://doi.org/10.1007/978-3-642-19902-8_47.

Sappa, G., Rossi, M., Coviello, M.T., 2005. Effetti ambientali del sovrasfruttamento degli acquiferi della Pianura Pontina (Lazio). In: Proceedings of the Aquifer Vulnerability and Risk 2nd International Workshop. Parma, Italy, pp. 14–16.

Sappa, G., Barbieri, M., Ergul, S., Ferranti, F., 2012. Hydrogeological conceptual model of groundwater from carbonate aquifers using environmental isotopes (^{18}O, ^{2}H) and chemical tracers: a case study in Southern Latium Region, Central Italy. J. Water Resour. Prot. 4, 695–716. https://doi.org/10.4236/jwarp.2012.49080.

Sappa, G., Ergul, S., Ferranti, F., 2014. Water quality assessment of carbonate aquifers in southern Latium region, Central Italy: a case study for irrigation and drinking purposes. Appl. Water Sci. 4, 115–128. https://doi.org/10.1007/s13201-013-0135-9.

Sappa, G., Vitale, S., Ferranti, F., 2018. Identifying karst aquifer recharge areas using environmental isotopes: a case study in central Italy. Geosciences 8 (9), 351. https://doi.org/10.3390/geosciences8090351.

Saroli, M., Lancia, M., Albano, M., Casale, A., Giovinco, G., Petitta, M., Zarlenga, F., Dell'Isola, M., 2017. A hydrogeological conceptual model of the Suio hydrothermal area (central Italy). Hydrogeol. J. 25 (6), 1811–1832. https://doi.org/10.1007/s10040-017-1549-5.

Saroli, M., Albano, M., Giovinco, G., Casale, A., Dell'Isola, M., Lancia, M., Petitta, M., 2019. A macroscale hydrogeological numerical model of the Suio hydrothermal system (Central Italy). Geofluids 2019. https://doi.org/10.1155/2019/5485068.

Schettino, O., 1999. Analisi chimiche e batteriologiche dei pozzi A e B. In: Regione Lazio, Comune di Latina, Concessione Mineraria Terme di Fogliano, Università degli Studi di Napoli Federico II. Dipartimento di Chimica Farmaceutica e Tossicologia.

Schmid, S.M., Fügenschuh, B., Kounov, A., Maţenco, L., Nievergelt, P., Oberhänsli, R., Pleuger, J., Schefer, S., Schuster, R., Tomljenović, B., Ustaszewski, K., Van Hinsbergen, D.J., 2020. Tectonic units of the Alpine collision zone between Eastern Alps and western Turkey. Gondwana Res. 78, 308–374. https://doi.org/10.1016/j.gr.2019.07.005.

Schoeller, H., 1962. Les eaux souterraines. In: Hydrologie dynamique et chimique, Recherche, Exploitation et Évaluation des Ressources. Masson et Cie, Paris, 642pp.

Serva, L., Brunamonte, F., 2007. Subsidence in the Pontina plain. Italy. Bull. Eng. Geol. Environ. 66 (2), 125–134. https://doi.org/10.1007/s10064-006-0057-y.

Servizio Geologico d"Italia, 2010. Carta Geologica d'Italia alla scala 1:50.000, F. 402 Ceccano. ISPRA, Roma. https://www.isprambiente.gov.it/Media/carg/note_illustrative/402_Ceccano.pdf.

Sevink, J., van Gorp, W., Di Vito, M.A., Arienzo, I., 2020. Distal tephra from Campanian eruptions in early Late Holocene fills of the Agro Pontino graben and Fondi basin (Southern Lazio, Italy). J. Volcanol. Geotherm. Res. 405, 107041 https://doi.org/10.1016/j.jvolgeores.2020.107041.

Smedley, P.L., Kinniburgh, D.G., 2017. Molybdenum in natural waters: a review of occurrence, distributions and controls. Appl. Geochem. 84, 387–432. https://doi.org/10.1016/j.apgeochem.2017.05.008.

Smeraglia, L., Berra, F., Billi, A., Boschi, C., Carminati, E., Doglioni, C., 2016. Origin and role of fluids involved in the seismic cycle of extensional faults in carbonate rocks. Earth Planet. Sci. 450, 292–305. https://doi.org/10.1016/j.epsl.2016.06.042.

Stoppa, F., Cundari, A., 1995. A new Italian carbonatite occurrence at Cupaello (Rieti) and its genetic significance. Contrib. Mineral. Petrol. 122 (3), 275–288. https://doi.org/10.1007/s004100050127.

Taniguchi, M., Wang, K., Gamo, T., 2003. Land and Marine Hydrogeology. Elsevier, 0-444-51479-1.

Tavani, S., Granado, P., Corradetti, A., Camanni, G., Vignaroli, G., Manatschal, G., Mazzoli, S., Muñoz, J.A., Parente, M., 2021. Rift inheritance controls the switch from thin-to thick-skinned thrusting and basal décollement re-localization at the subduction-to-collision transition. GSA Bull. 133 (9–10), 2157–2170. https://doi.org/10.1130/B35800.1.

Tavani, S., Smeraglia, L., Fabbi, S., Aldega, L., Sabbatino, M., Cardello, G.L., Maresca, A., Schirripa Spagnolo, G., Kylander-Clark, A., Billi, A., Bernasconi, S.M., Carminati, E., 2023. Timing, thrusting mode, and negative inversion along the Circeo thrust, Apennines, Italy: how the accretion-to-extension transition operated during slab rollback. Tectonics 42 (6), e2022TC007679. https://doi.org/10.1029/2022TC007679.

Torresan, F., Piccinini, L., Pola, M., Zampieri, D., Fabbri, P., 2020. 3D hydrogeological reconstruction of the fault–controlled Euganean Geothermal System (NE Italy). Eng. Geol. 274, 105740 https://doi.org/10.1016/j.enggeo.2020.105740.

Trumpy, E., Manzella, A., 2017. Geothopica and the interactive analysis and visualization of the updated Italian National Geothermal Database. Int. J. Appl. Earth Obs. Geoinf. 54, 28–37. https://doi.org/10.1016/j.jag.2016.09.004.

Tuccimei, P., Salvati, R., Capelli, G., Delitala, M.C., Primavera, P., 2005. Groundwater fluxes into a submerged sinkhole area, Central Italy, using radon and water chemistry. Appl. Geochem. 20 (10), 1831–1847. https://doi.org/10.1016/j.apgeochem.2005.04.006.

van Stempvoort, D.R., Krouse, H.R., 1994. Controls of $\delta^{18}O$ in sulfate: review of experimental data application to specific environments. In: Alpers, C.A., Blowes, D. W. (Eds.), Environmental Geochemistry of Sulfide Oxidation. Am. Chem. Soc, Washington DC, pp. 446–480. https://doi.org/10.1021/bk-1994-0550.ch029.

Vespasiano, G., Marini, L., Muto, F., Auqué, L.F., Cipriani, M., De Rosa, R., Critelli, S., Gimeno, M.J., Blasco, M., Dotsika, E., Apollaro, C., 2021. Chemical, isotopic and geotectonic relations of the warm and cold waters of the Cotronei (Ponte Coniglio), Bruciarello and Repole thermal areas (Calabria-Southern Italy). Geothermics 96, 102228. https://doi.org/10.1016/j.geothermics.2021.102228.

Wang, J., Jin, M., Jia, B., Kang, F., 2015. Hydrochemical characteristics and geothermometry applications of thermal groundwater in northern Jinan, Shandong, China. Geothermics 57, 185–195. https://doi.org/10.1016/j.geothermics.2015.07.002.

WHO, 2022. Guidelines for Drinking-Water Quality Fourth Edition Incorporating the First and Second Addenda. World Health Organization, Geneva, Switzerland.

Yang, P., Luo, D., Hong, A., Ham, B., Xie, S., Ming, X., Wang, Z., Pang, Z., 2019. Hydrogeochemistry and geothermometry of the carbonate-evaporite aquifers controlled by deep-seated faults using major ions and environmental isotopes. J. Hydrol. 579, 124116 https://doi.org/10.1016/j.jhydrol.2019.124116.

Zhang, W., Xiong, K., Li, Y., Song, S., Xiang, S., 2024. Improving grassland ecosystem services for human wellbeing in the karst desertification control area: anthropogenic factors become more important. Sci. Total Environ. 946 (15), 174199 https://doi.org/10.1016/j.scitotenv.2024.174199.